

# Early Defect Identification for Micro LED Displays via Photoluminescent and Cathodoluminescent Imaging

Keith Behrman  
PhD candidate, Electrical Engineering  
Columbia University, New York  
New York, NY USA  
keith.behrman@columbia.edu

Julie Fouilloux  
Graduate Student, Chemical Engineering  
Brunel University London  
London UK  
julie.fouilloux@enscm.fr

Terry Ireland  
Research Fellow, Chemical Engineering  
Brunel University London  
London UK  
Terry.Ireland@brunel.ac.uk

George R Fern  
Theme Leader / Reader, Chemical Engineering  
Brunel University London  
London UK  
George.Fern@brunel.ac.uk

Jack Silver  
Professor, Chemical Engineering  
Brunel University London  
London UK  
Jack.Silver@brunel.ac.uk

Ioannis Kymissis  
Professor, Electrical Engineering  
Columbia University, New York  
Principal Engineer, Lumiode  
New York, NY USA  
johnkym@ee.columbia.edu

This is the author manuscript accepted for publication and has undergone full peer review but has not been through the copyediting, typesetting, pagination and proofreading process, which may lead to differences between this version and the [Version of Record](#). Please cite this article as doi: [10.1002/jsid.985](https://doi.org/10.1002/jsid.985)

## Abstract

Ultra-high resolution micro light emitting diode (LED) displays are emerging as a viable technology for self-emissive displays. Several of the critical issues facing micro LED displays with millions of pixels are fidelity, process control, and defect analysis during LED fabrication and transfer. Here, we investigate two non-destructive test methods, photoluminescent and cathodoluminescent imaging, and compare them to electroluminescent images to verify LED fidelity and evaluate these methods as potential tools for defect analysis. We show that utilizing cathodoluminescent imaging as an analysis tool provides a rich data set that can identify and categorize common defects during micro LED display fabrication that correspond to electroluminescence. Photoluminescent imaging, however, is not an effective method for fidelity analysis but does provide information on dry etching uniformity.

## Keywords

Micro LED; photoluminescence; cathodoluminescence; pixel transfer; defect analysis; quality control.

## 1 Introduction

Micro light-emitting diodes (micro LEDs) are a promising technology for next-generation displays given their high brightness and efficiency, color gamut coverage, and self-emissive design [1, 2, 3]. Several HD and UHD displays have been demonstrated as prototypes, but there have been few commercial micro LED displays [4, 5]. Most applications require red, green, and blue (RGB) pixel integration, which is currently not possible from a single epitaxially-grown LED wafer in a fully self-emissive design [6]. Green and blue emission are both typically from GaN epitaxial stacks with an  $\text{In}_x\text{Ga}_{1-x}\text{N}$  emissive layer where the indium alloy content dictates the bandgap [7]. The best performing red-emissive devices, however, come from InGaAs epitaxial stacks [8]. The inherent difficulties in integrating these different epitaxial stacks onto a single display backplane for RGB integration have spurred numerous research efforts to a solution that is both cost-effective and robust. Green and blue emission with monolithic integration has been shown by utilizing two emissive layers, the quantum confined Stark effect, and strain modulation [9, 10, 11]. Fundamental differences in the growth methods and substrate requirements of InGaN and InGaAs complicates monolithic integration, with selective area epitaxy through nanowire growth being a notable exception [12].

To overcome this limitation, several transfer methods have been proposed to allow integration of singulated micro LEDs from red, green, and blue LED wafers onto a single wafer or backplane [3, 13, 14, 15, 16]. Given the 8.3 million pixels in an ultra-high-definition (UHD) display, these transfer methods can require up to 25 million micro LED transfers per display for RGB integration. The high number of transfers require 99.999999 % yield throughout the entire fabrication process to produce displays with a 75% final yield with no inactive pixels. Lesser fabrication yields result in a higher percentage of displays with inactive pixels, requiring the display to either be discarded or repaired [17]. Both add to the total fabrication cost of the display, and the latter may not be possible depending on the device architecture.

Inactive pixels can result from many defect mechanisms throughout the fabrication process. For instance, transfers can fail due to LED damage during the transfer process or improper seating of the LED to the backplane. In addition, improper passivation of the LED sidewalls can result in short-circuits between the cathode and anode, and chlorine-based dry etching-related damage

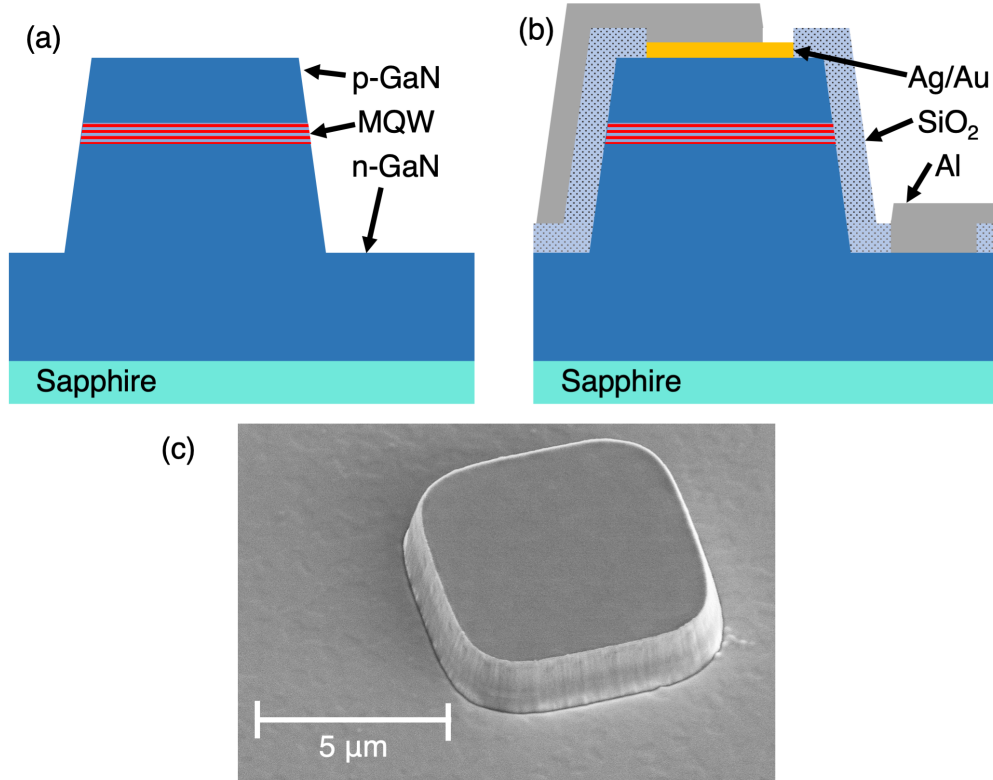


Figure 1: Device design. (a) Cross-section schematic of a single LED after dry etching. (b) Cross-section schematic of a single LED after passivation and metal wiring. (c) SEM image of a  $5 \times 5 \mu\text{m}^2$  LED after dry etching the mesa structure as depicted in Fig. 1a. [18].

to the LED during mesa formation or redeposited GaN/GaAs related compounds can also cause short-circuits [19, 20, 21]. Defects in the wiring or interconnects can also cause inactive pixels. For many of these defects, the primary method of defect analysis is electroluminescent (EL) imaging and optical quality assurance checks [22, 23]. Unfortunately, this cannot be performed until the display is fully assembled and then must either be discarded or repaired. A non-destructive method to examine for pixel damage would significantly improve yield and fabrication quality while reducing manufacturing costs. Photoluminescent (PL) imaging has been utilized as a metrology and diagnostic tool for semiconductor devices to characterize photoemission and charge carrier properties [24, 25, 26, 27]. It has also been utilized as a defect diagnostic tool for semiconductor devices, poising it as a promising methodology for defect detection in micro LEDs. [28]. Cathodoluminescent (CL) imaging is similarly a useful imaging tool for mapping bandgap properties of nano and low-dimensional devices [29, 30, 31]. Here we investigate the viability of PL and CL imaging as two non-destructive test methods for short-circuit related defects in micro LED displays.

## 2 Experimental methods and fabrication

We used commercially available blue LED wafers (448 nm center wavelength) of epitaxially grown GaN and InGaN on micro-patterned sapphire for this study. The epitaxial growth stack consists of undoped GaN, n-type GaN, multiple quantum wells (MQWs), and p-type GaN. Each quantum well contains a few nm thick InGaN emissive region contained between undoped GaN

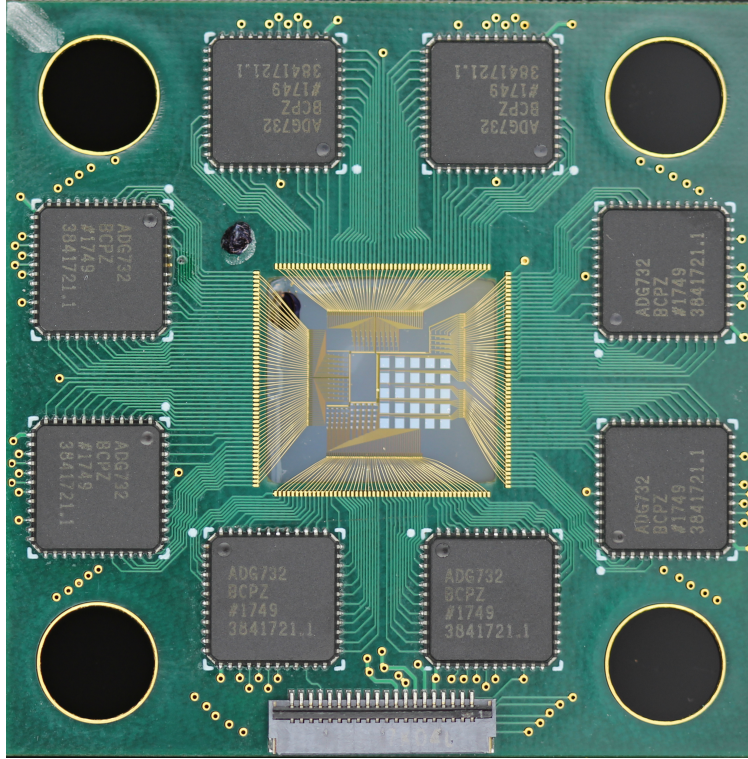


Figure 2: Multiplexer PCB with attached and wirebonded die for EL imaging [18].

barriers. Wafers were first thinned by mechanical grinding to approximately  $200\ \mu\text{m}$  thick and stealth diced into  $10\times 10\ \text{mm}^2$  dies for processing. Each die was then coated with  $500\ \text{nm}$  of PECVD  $\text{SiO}_2$  to be used as a hard mask during LED formation. The  $\text{SiO}_2$  was coated with LOR 5A and S1805 for a bi-layer resist lift-off process. The resist was patterned using a DWL 66+ in direct writing mode to produce 200 square LEDs per die with side lengths of 5, 10, 15, 20, 25, 50, 100, and  $500\ \mu\text{m}$ . There are 25 of each LED size per die.  $50\ \text{nm}$  of chrome was e-beam deposited and lifted off in a solvent bath. The  $\text{SiO}_2$  hard masks were patterned in an Oxford 100 dry etcher using  $\text{CHF}_3$  and argon gases. The remainder of the chrome was wet etched before GaN etching to prevent contamination of the LED sidewalls from redeposited chrome. The GaN was then dry etched using a mixture of  $\text{Cl}_2$  and  $\text{BCl}_3$  to a depth of  $1100\ \text{nm}$  to expose the n-GaN layer below the MQWs. The remainder of the  $\text{SiO}_2$  was wet etched in 10:1 buffered oxide etchant (BOE). The samples were then cleaned with acetone and oxygen plasma before imaging. Fig. 1 shows a schematic and an SEM image of a pixel.

CL images were taken using a Zeiss Supra 35VP field-emission scanning electron microscope (FESEM). Images were taken using the secondary electron (SE) detector and a photomultiplier tube. Samples were fixed to a stub with the n-GaN electrically connected to ground via conductive carbon tape. The SE detector was used to locate and verify the LED structures and the photomultiplier tube detector was used to collect the CL images. Engelsen et al., have detailed this method in more detail here [32].

PL images were recorded using a LEICA SP8 stimulated emission depletion microscope. The excitation source was a  $405\ \text{nm}$  diode laser programmed to raster scan over the active area of the die. The  $405\ \text{nm}$  laser line is sufficiently powerful enough to excite electrons to the conduction band in the InGaN wells but does not excite the wider bandgap GaN. Images were acquired from the

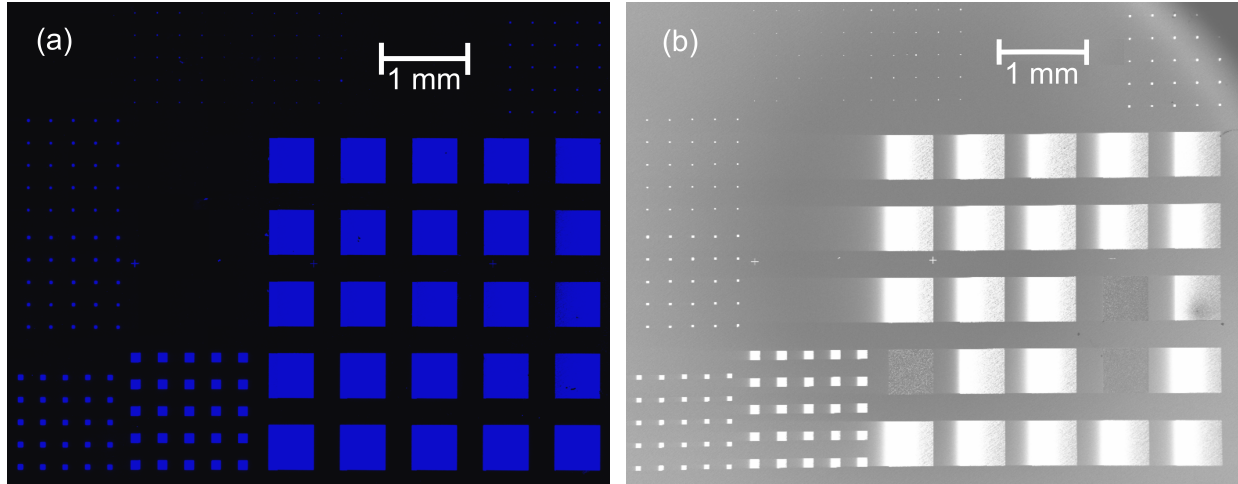


Figure 3: Non-destructive images. (a) PL composite image of 200 LEDs. Several images were stitched together to cover the entire device area. All LEDs are illuminated in this image. (b) CL SEM image of the same 200 LEDs from (a). While most LEDs exhibit emission, several are inactive [18].

photomultiplier tube sensor with a bandpass filter set between 425 and 475 nm to remove excitation source reflections and background noise. For both images, the number and location of the inactive pixels were recorded.

After both non-destructive images were collected, we continued device fabrication to compare these methods with EL imaging. First the samples were cleaned in Nanostrip followed by acetone, IPA, and DI water baths to remove any contamination from adhesive residue used in imaging. PECVD  $\text{SiO}_2$  was deposited on the samples as a passivation layer. The  $\text{SiO}_2$  was dry-etched with a photoresist mask to expose the n-type and p-type GaN layers for electrical contact. A bi-layer resist stack of LOR 30B and SPR220 4.5 was spin-coated and patterned for lift-off of 20 nm silver / 60 nm gold ohmic contacts to the p-GaN. After stripping the remaining photoresist, 300 nm of conformal sputtered aluminum was lifted off with the same bilayer stack to contact the n-GaN and to connect each p-GaN contact over the LED sidewall. Each pixel was addressed individually while using a common n-GaN contact instead of passive matrix addressing to prevent an entire row or column of pixels to be inactive from a single short circuit defect. Individual wiring, while more tedious, gives higher precision to the exact location of a defect. The samples were deposited with 5 nm chromium / 600 nm gold and lifted off to form wire bond pads at each contact. Finally, the samples were fixed to a printed circuit board (PCB) with adhesive and wire-bonded with a semi-automatic bonder. The finished device is shown in Fig. 2. The PCB contains multiplexers to address each LED controlled by a Teensy 3.6 microcontroller. The Teensy firmware programmed the current output from a Keithly 2410 source meter unit to each LED subarray of 25 devices. EL images were taken under a 5x microscope to verify device illumination. The inactive pixels were counted and compared to their respective PL and CL images.

After EL analysis, additional CL images were taken with the die still attached to the PCB. The common n-GaN contact was electrically connected to the stub of the SEM through a test point contact on the PCB. The individual p-GaN contacts were connected through the wirebonds to the inactive multiplexer integrated circuits (ICs) acting as a virtual ground current return path for the incident electrons. This provides a new measurement paradigm allowing multiple current return paths that results in images with a richer dataset.

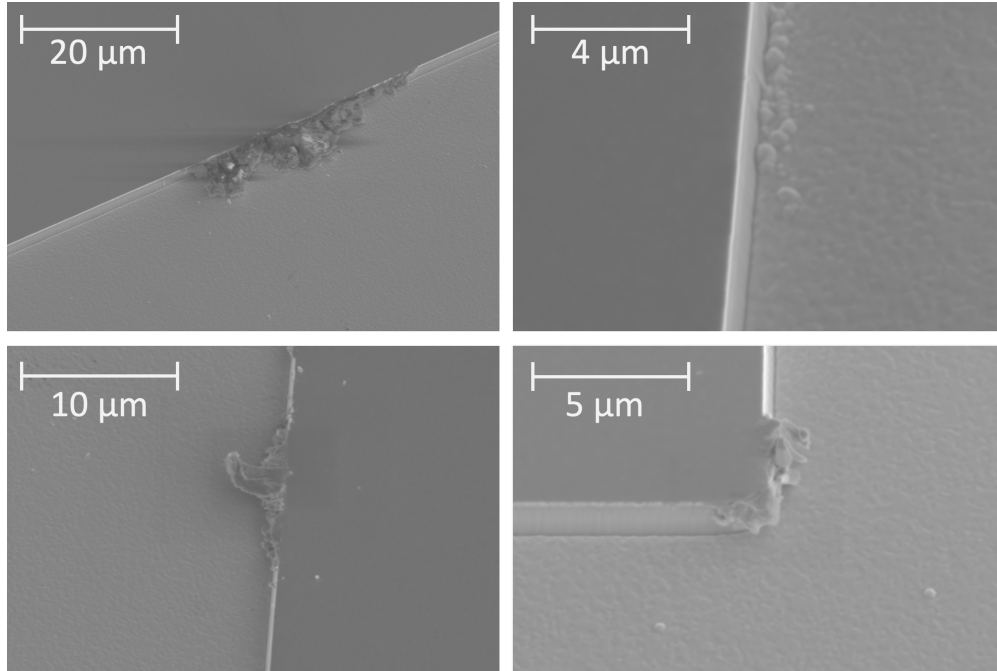


Figure 4: SEM images of pixel damage from dry etching [18].

### 3 Results and Discussion

The PL images show emission centered around 448 nm at the locations of the formed LEDs. An example PL image can be seen in Fig. 3a. The image shows 200 LEDs in a  $6 \times 5 \text{ mm}^2$  area. All 200 LEDs exhibit PL in this image. Note that the  $5 \times 5$ ,  $10 \times 10$  and  $15 \times 15 \text{ μm}^2$  pixels in the top row are all active but are difficult to see at this scale. We also observed illumination at the alignment marks and from scattered spots and defects throughout the die, even at locations far from the pixel structures. The scattered spots are composed of InGaN material that have either been created as particles from handling or areas of re-sputtered InGaN from the etching process. This shows that PL imaging can provide some information on dry-etching uniformity by analyzing PL emission outside of desired micro LED locations. Across the four individual dies, all 800 pixels exhibited PL after the dry etching step. This does not mean that PL imaging is predicting 100% yield but instead is an ineffective predictor of dry-etching related defects as first reported by Tesoro Scientific [22, 23]. This is further supported by CL and EL results discussed next that show lesser yields. We pose that PL excitation is not affected by short-circuit defects across the etched LED sidewall because of the lack of carrier transport. Electrons within the InGaN quantum wells are excited by the 405 nm light and show emission upon relaxation regardless of the presence of a short-circuit.

The CL images are panchromatic and are thus insensitive to spectra but display qualitative luminescent intensity. Quantitative comparisons between wafers or dies would be possible in a calibrated system but was not available due to image acquisition occurring over several days with multiple users. Fig. 3b shows an example image of the same die that is displayed in Fig. 3a. The areas in bright white represent strong luminescence. An LED with little or no luminescence is indicative of a defect causing an electrical short between the anode and cathode providing a shunt resistance current return path around the emissive InGaN MQWs. Otherwise, electrons injected from the FESEM's gun would return to ground through the InGaN layer and emission would be observed.

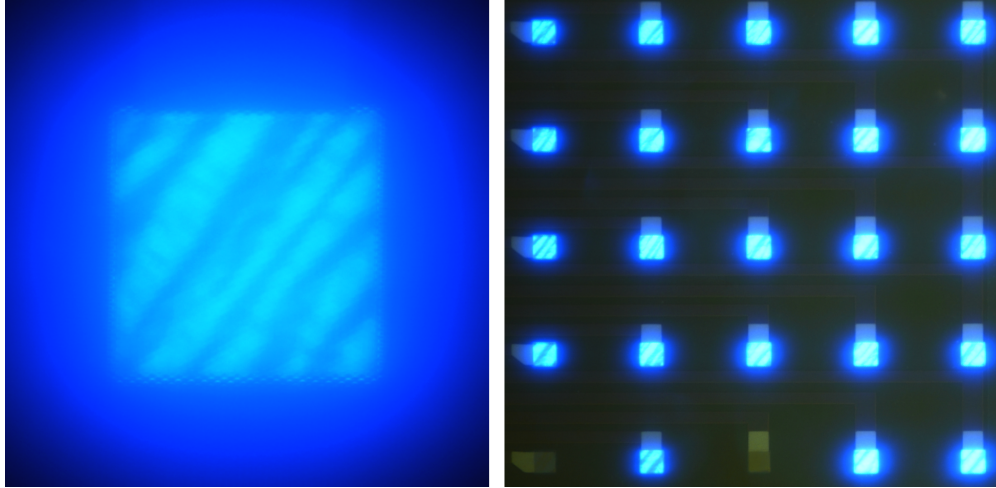


Figure 5: Electroluminescent images of a single  $50 \times 50 \mu\text{m}^2$  pixel and an array of  $50 \times 50 \mu\text{m}^2$  pixels [18].

We explored this phenomenon further by examining the edges of the inactive pixels under SEM with an SE detector. We were able to find various defects likely related to re-deposited material or micro-masking from defects in the  $\text{SiO}_2$  etch or photoresist residue. Example SEM images of the defects can be seen in Fig. 4.

We recorded EL images of all pixels amongst all four dies. Fig. 5 shows example images of a single pixel and an array with both active and inactive pixels. Darkfield images were taken with the PCB mounted underneath a microscope objective focusing through the sapphire, also referred to as bottom emission. The EL active pixels have a distinct non-uniformity with a scattered bloom around the edges of emission. The non-uniformity is likely due to surface roughness variations caused from sapphire grinding during the thinning process. The scattered bloom is a result of the scattering microstructures built into the sapphire substrate. We compared the yield results from CL to EL to better understand their relationship. Pixels were examined as being active (luminescent) or inactive (non-luminescent) for both tests. Given this, there are four distinct pixel outcomes when compared with CL imaging:

- Active both with CL and EL - 71.75% of samples. This was the most common outcome and suggests that CL is an accurate predictor of EL performance.
- Active with CL but inactive with EL - 24.25% of samples. This was the second most common result and suggests no dry-etching-related damage, and further processing after CL imaging introduced additional defects, preventing EL.
- Inactive both with CL and EL - 3% of samples. This outcome suggests that a short-circuit defect was introduced during the dry etching stage of device fabrication and that CL is an accurate predictor of EL results from etching related damage.
- Inactive with CL but active with EL - 1% of samples. This was the least common result and suggests that nanostrip cleaning removed some etching-related damage, or that the sidewall passivation process inadvertently modified the surface to increase the shunt resistance. This is expected as sidewall passivation and chemical treatments have been shown to improve device performance [33, 34].

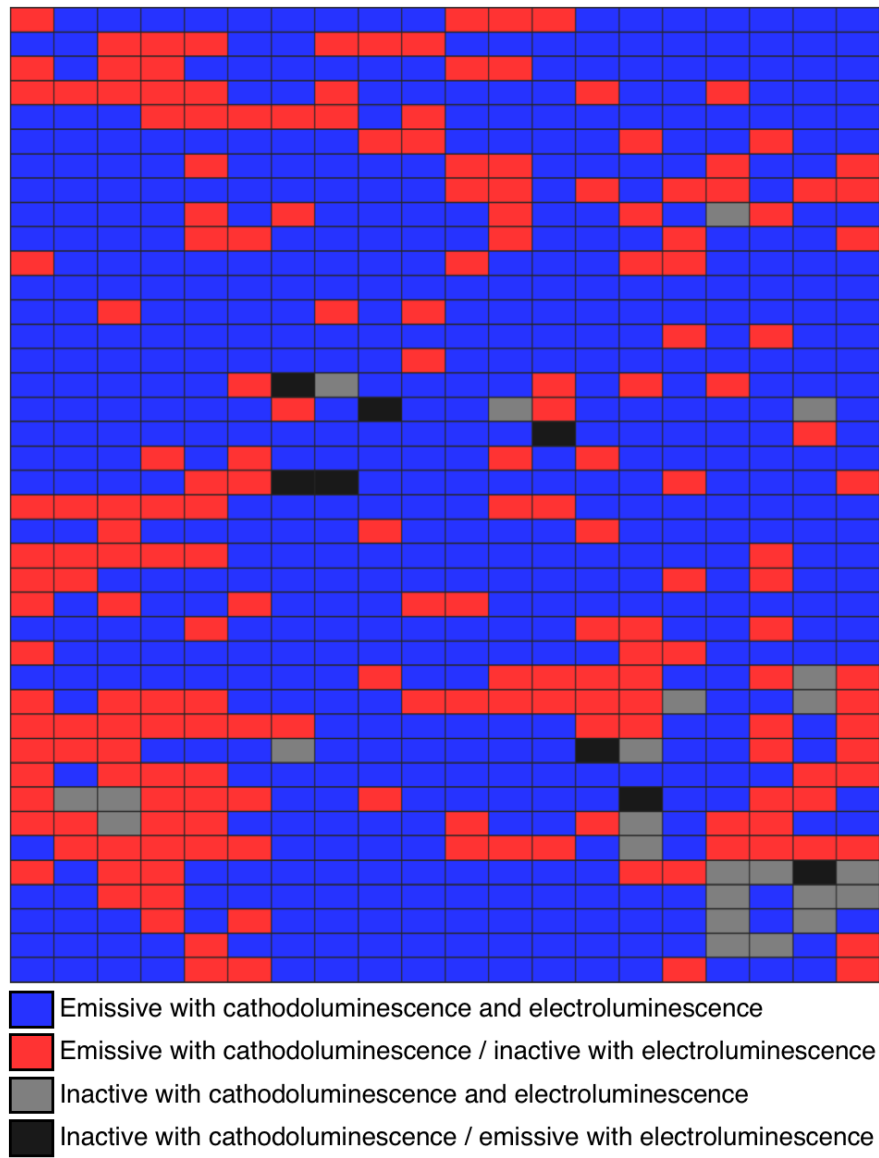


Figure 6: Heatmap of the yield results from all 800 examined pixels comparing the results of cathodoluminescence and electroluminescence [18].



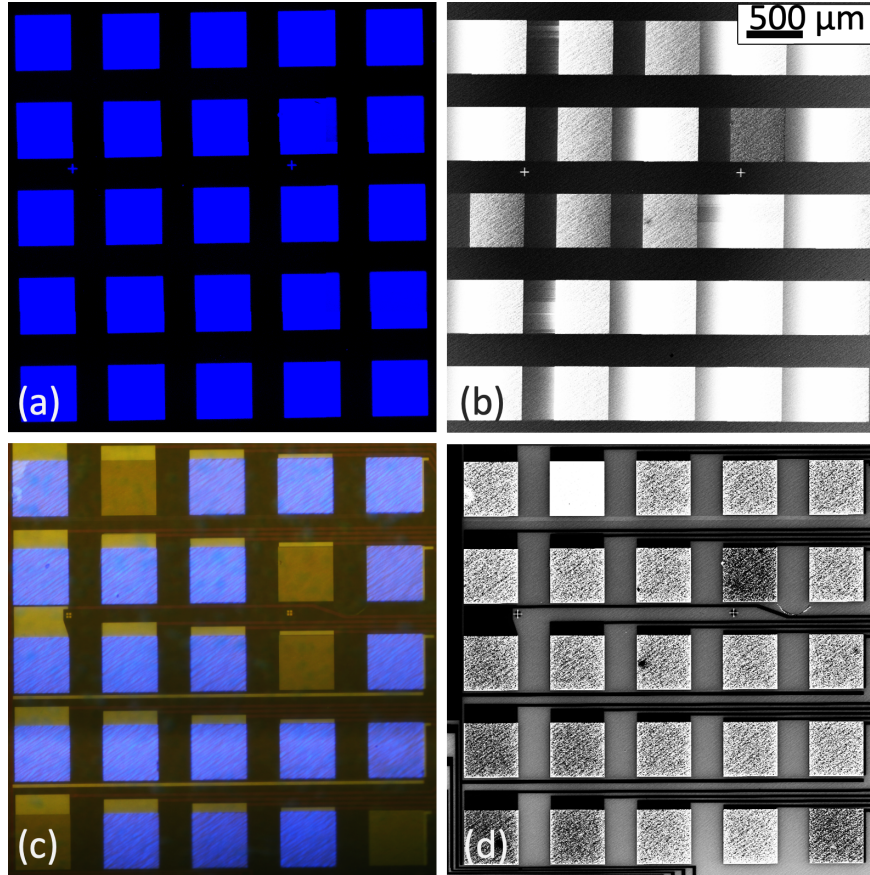


Figure 7: Twenty-five  $500 \times 500 \mu\text{m}^2$  pixel images. (a) PL image after mesa etch. (b) CL image after mesa etch. (c) EL image after completed fabrication and die attach. (d) CL image after completed fabrication and die attach.

A summary of all of these outcomes is mapped in Fig. 6. All pixels were active in PL tests but these results were not consistent for CL and EL imaging. For this reason, PL results were not compared in Fig. 6.

The second most common result, active with CL but inactive with EL, can be explained due to the difficulty in handling small dies through several fabrication steps thus introducing further defects. Additionally, there was visible conductive adhesive residue from fixing the samples to the SEM chuck that was difficult to remove with further chemical processing that contaminated large numbers of pixels. These contaminated pixels were predominately inactive with EL imaging. Defects in the wiring of the pixels also caused EL failure.

We reexamined a subset of the devices with CL imaging with the die attached to the PCB. This represents a new measurement paradigm as the incident electrons from the FESEM gun are now being absorbed by the p-GaN metal contact rather than the p-GaN itself. With the contact metal at a higher potential, the path electrons use to return to a lower potential state depends on the defect state of each pixel.

To highlight this phenomenon, Fig. 7 shows twenty-five pixels with four non-destructive images. The PL images in Fig. 7a show uniform luminescence and predict no defects in this array. The CL images in Fig. 7b display a variety of contrast levels which we interpret as a reliability marker for a short circuit related defect for etching related damage. The majority of the pixels show very bright

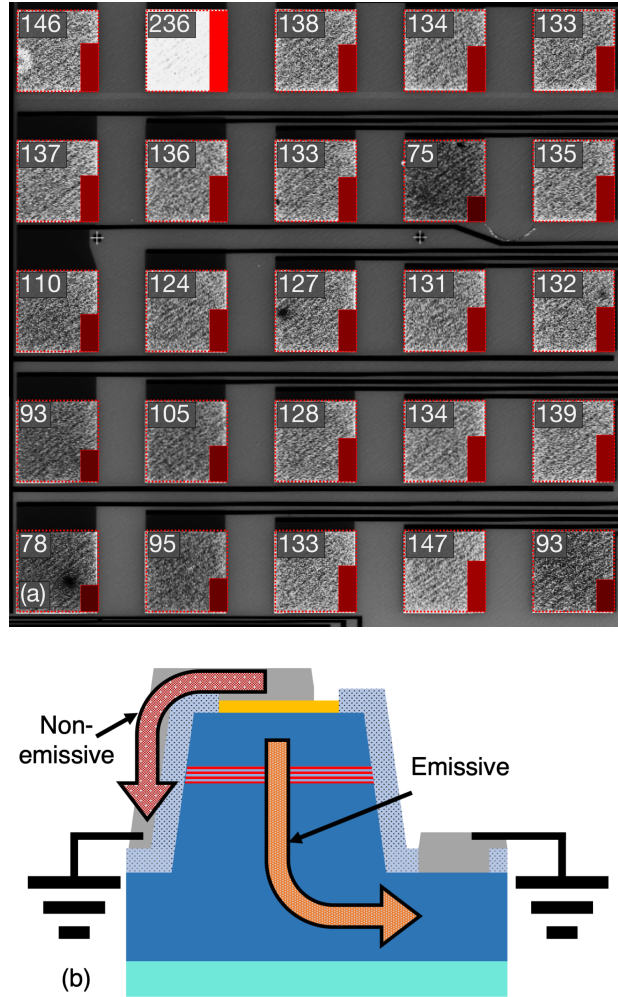


Figure 8: (a) Brightness analysis of CL data from the pixels in Fig. 7d. (b) Current return paths for incident electrons during CL imaging.

luminescence, predictive of no damage. Several pixels show intermediate brightness and one pixel shows very low brightness. The blurring effect seen is due to the long carrier lifetime in the InGaN MQWs and short pixel integration time as described in detail by Engelsen [32]. When compared to the EL image in Fig. 7c, we observe five defective pixels where only one defect is correctly predicted by CL imaging before fabrication completion, indicated by the low-brightness pixel.

Comparing CL images in Fig. 7b and d show stark differences in pixel illumination. One pixel in Fig. 7d is distinctly brighter than the remaining pixels. Most are of intermediate brightness and a few have diminished luminescence. Compared to the known defective pixels from Fig. 7c, we see that the brightest pixel and three of the dimmest pixels in Fig. 7d correspond to defects. One discrepancy is the dead pixel in the middle row of Fig. 7c does not seem to be predicted by either CL image.

To quantify the intensity of each pixel from Fig. 7d, we devised a simple script in MATLAB to measure the brightness of each pixel from marked regions of interest (ROI) as seen in Fig. 8a. The average intensity of all pixels within each ROI is overlaid on the pixel within a range from 0 to 255. These brightness values provide accurate predictions on the luminescent properties under EL and the defect state of each pixel. Pixels near the maximum brightness range indicate high amounts of

optical recombination occurring in the InGaN, suggesting a minimum amount of current returning through the p-GaN contact to a virtual ground as represented in Fig. 8b. This suggests a defect in wiring or attachment to the p-GaN contact, as seen by a lack of luminescence in Fig. 7c. Pixels near the minimum brightness range indicate low amount of optical recombination suggesting a minimum amount of emissive current. This suggests either a shunt resistance across the emissive InGaN or a wiring defect with the n-GaN contact or wiring. Pixels sitting in the middle of the brightness range suggest utilization of both current return paths with no shunt resistance from dry-etching damage. The majority of the pixels fall within this range and correlate to the luminescent pixels in Fig. 7c.

Fig. 7 and 8 demonstrate the feasibility of accurate defect analysis of micro LEDs utilizing CL imaging. We demonstrated this technology with small batch devices fabricated in a university cleanroom with shared equipment. CL analysis was performed in a conventional FESEM with a photomultiplier detector and a semi-automated MATLAB script. We believe that scaling CL technology to wafer or panel sized fabrication equipment with automated image analysis would be a reliable technique for defect analysis in industrial mass production of micro LEDs.

## 4 Conclusion

Self-emissive micro LED displays still exist as an expensive and specific solution for niche applications due to the difficulty in producing displays with millions of pixels, with no inactive LEDs, and integrating multiple colors onto one backplane. By utilizing CL imaging, micro LED short-circuit defects from dry-etching-related damage causing individual pixels or LEDs to become inactive under EL can be reliably predicted. PL imaging can identify re-deposited InGaN from etching processes that could hinder further fabrication process steps. However, PL imaging fails to identify etching related damage causing LED short circuits. Additional wiring and contact defects are simply identified via CL imaging and brightness measurements. These two methods of CL pose as fast and non-destructive measurements to provide fidelity information for micro LED displays.

## 5 Acknowledgements

This work was carried out in part in the Clean room / Electron Microscopy / Shared Materials Characterization/ lab of Columbia Nano Initiative (CNI) Shared Lab Facilities at Columbia University. This study was supported by NSF grant 1926747 and NIH grant 5R21EY029458-02. We would like to thank Magic Leap for providing additional grant funding to sponsor this project.

## 6 Competing financial interest

Ioannis Kymissis is a board member of Lumiode, which is a start-up working in micro LED and holds an equity stake in the company.

## References

- [1] Wu T, Sher CW, Lin Y, Lee CF, Liang S, Lu Y, et al. Mini-LED and Micro-LED: Promising Candidates for the Next Generation Display Technology. *Applied Sciences*. 2018 Sep;8(9):1557.
- [2] Um JG, Jeong DY, Jung Y, Moon JK, Jung YH, Kim S, et al. Active-Matrix GaN -LED Display Using Oxide Thin-Film Transistor Backplane and Flip Chip LED Bonding. *Advanced Electronic Materials*. 2019;5(3):1800617.

- [3] Cok RS, Meitl M, Rotzoll R, Melnik G, Fecioru A, Trindade AJ, et al. Inorganic light-emitting diode displays using micro-transfer printing: LED displays using micro-transfer printing. *Journal of the Society for Information Display*. 2017 Oct;25(10):589–609.
- [4] Zhao Jun Liu, Wing Cheung Chong, Ka Ming Wong, Kei May Lau. 360 PPI Flip-Chip Mounted Active Matrix Addressable Light Emitting Diode on Silicon (LEDoS) Micro-Displays. *Journal of Display Technology*. 2013 Aug;9(8):678–682.
- [5] Chong WC, Cho WK, Liu ZJ, Wang CH, Lau KM. 1700 Pixels Per Inch (PPI) Passive-Matrix Micro-LED Display Powered by ASIC. In: 2014 IEEE Compound Semiconductor Integrated Circuit Symposium (CSICS). La Jolla, CA, USA: IEEE; 2014. p. 1–4.
- [6] Templier F, Dupré L, Tirano S, Marra M, Verney V, Olivier F, et al. 75-1: Invited Paper: GaN-based Emissive Microdisplays: A Very Promising Technology for Compact, Ultra-high Brightness Display Systems. *SID Symposium Digest of Technical Papers*. 2016;47(1):1013–1016.
- [7] Nakamura S, Senoh M, Iwasa N, Nagahama Si. High-Brightness InGaN Blue, Green and Yellow Light-Emitting Diodes with Quantum Well Structures. *Japanese Journal of Applied Physics*. 1995 Jul;34(Part 2, No. 7A):L797–L799.
- [8] Schubert EF. *Light-Emitting Diodes*. 2nd ed. Cambridge University Press; 2006.
- [9] Damilano B, Grandjean N, Pernot C, Massies J. Monolithic White Light Emitting Diodes Based on InGaN/GaN Multiple-Quantum Wells. *Japanese Journal of Applied Physics*. 2001 Sep;40(Part 2, No. 9A/B):L918–L920.
- [10] Ozden I, Makarona E, Nurmikko AV, Takeuchi T, Krames M. A dual-wavelength indium gallium nitride quantum well light emitting diode. *Applied Physics Letters*. 2001 Oct;79(16):2532–2534.
- [11] Ryou JH, Lee W, Limb J, Yoo D, Liu JP, Dupuis RD, et al. Control of quantum-confined Stark effect in InGaNGaN multiple quantum well active region by p-type layer for III-nitride-based visible light emitting diodes. *Applied Physics Letters*. 2008 Mar;92(10):101113.
- [12] Chul-Ho Lee, Young Joon Hong, Yong-Jin Kim, Jinkyong Yoo, Hyeonjun Baek, Seong-Ran Jeon, et al. GaN/ZnO Nanotube Heterostructure Light-Emitting Diodes Fabricated on Si. *IEEE Journal of Selected Topics in Quantum Electronics*. 2011 Jul;17(4):966–970.
- [13] Carlson A, Bowen AM, Huang Y, Nuzzo RG, Rogers JA. *Transfer Printing Techniques for Materials Assembly and Micro/Nanodevice Fabrication*. *Advanced Materials*. 2012 Oct;24(39):5284–5318.
- [14] Schuele PJ, Sasaki K, Ulmer K, Lee JJ; Inc. eLUX, assignee. DISPLAYWITH SURFACE-MOUNT EMISSIVE ELEMENTS. 9,825,202; 2017.
- [15] Bibl A, Higginson JA, Clara S, Law HFS, Hu HH; LuxVue Technology Corporation, assignee. METHOD OF TRANSFERRING A MICRO DEVICE. US8,333,860B1; 2012.
- [16] Cheng DI, Rumpler JJ, Perkins JM, Zahn M, Fonstad CG, Cramer ES, et al. Use of patterned magnetic films to retain and orient micro-components during fluidic assembly. *Journal of Applied Physics*. 2009 Apr;105(7):07C123.

- [17] Meitl M, Radauscher E, Bonafede S, Gomez D, Moore T, Prevatte C, et al. 55-1: *Invited Paper*: Passive Matrix Displays with Transfer-Printed Microscale Inorganic LEDs. SID Symposium Digest of Technical Papers. 2016 May;47(1):743–746.
- [18] Behrman K, Fouilloux J, Ireland T, Fern GR, Silver J, Kymissis I. 37-4: Micro LED Defect Analysis via Photoluminescent and Cathodoluminescent Imaging. SID Symposium Digest of Technical Papers. 2020 Aug;51(1).
- [19] Kou J, Shen CC, Shao H, Che J, Hou X, Chu C, et al. Impact of the surface recombination on InGaN/GaN-based blue micro-light emitting diodes. Optics Express. 2019 Jun;27(12):A643.
- [20] Pearton SJ, Shul RJ, Ren F. A Review of Dry Etching of GaN and Related Materials. MRS Internet Journal of Nitride Semiconductor Research. 2000;5(1):e11.
- [21] Chang L, Yeh YW, Hang S, Tian K, Kou J, Bi W, et al. Alternative Strategy to Reduce Surface Recombination for InGaN/GaN Micro-light-Emitting Diodes—Thinning the Quantum Barriers to Manage the Current Spreading. Nanoscale Research Letters. 2020 Dec;15(1):160.
- [22] Henley FJ. Key Production Equipment Requirements to Realize High-Yield MicroLED Mass-Production. In: International Display Workshop. Nagoya, Japan; 2018. p. 4.
- [23] Henley FJ. 18-1: *Invited Paper*: Evaluating In-Process Test Compatibility of Proposed Mass-Transfer Technologies to Achieve Efficient, High-Yield MicroLED Mass-Production. SID Symposium Digest of Technical Papers. 2019 Jun;50(1):232–235.
- [24] Bao W, Melli M, Caselli N, Riboli F, Wiersma DS, Staffaroni M, et al. Mapping Local Charge Recombination Heterogeneity by Multidimensional Nanospectroscopic Imaging. Science. 2012 Dec;338(6112):1317–1321.
- [25] Bao W, Su Z, Zheng C, Ning J, Xu S. Carrier Localization Effects in InGaN/GaN Multiple-Quantum-Wells LED Nanowires: Luminescence Quantum Efficiency Improvement and “Negative” Thermal Activation Energy. Scientific Reports. 2016 Oct;6(1):34545.
- [26] Badcock TJ, Ali M, Zhu T, Pristovsek M, Oliver RA, Shields AJ. Radiative recombination mechanisms in polar and non-polar InGaN/GaN quantum well LED structures. Applied Physics Letters. 2016 Oct;109(15):151110.
- [27] Chen W, Wen X, Latzel M, Yang J, Huang S, Shrestha S, et al. Nanoscale characterization of GaN/InGaN multiple quantum wells on GaN nanorods by photoluminescence spectroscopy. San Francisco, California, United States; 2017. p. 101040U.
- [28] Sugimoto H, Araki K, Tajima M, Eguchi T, Yamaga I, Dhamrin M, et al. Photoluminescence analysis of intragrain defects in multicrystalline silicon wafers for solar cells. Journal of Applied Physics. 2007 Sep;102(5):054506.
- [29] Olivier F, Daami A, Dupré L, Henry F, Aventurier B, Templier F. 25-4: Investigation and Improvement of 10um Pixel-pitch GaN-based Micro-LED Arrays with Very High Brightness. SID Symposium Digest of Technical Papers. 2017 May;48(1):353–356.
- [30] Strunk HP, Albrecht M, Scheel H. Cathodoluminescence in transmission electron microscopy. Journal of Microscopy. 2006 Oct;224(1):79–85.

- [31] Ogletree DF, Schuck PJ, Weber-Bargioni AF, Borys NJ, Aloni S, Bao W, et al. Revealing Optical Properties of Reduced-Dimensionality Materials at Relevant Length Scales. *Advanced Materials*. 2015 Oct;27(38):5693–5719.
- [32] Engelsen DD, Harris PG, Ireland TG, Fern GR, Silver J. Contrast and decay of cathodoluminescence from phosphor particles in a scanning electron microscope. *Ultramicroscopy*. 2015 Oct;157:27–34.
- [33] Wong MS, Hwang D, Alhassan AI, Lee C, Ley R, Nakamura S, et al. High efficiency of III-nitride micro-light-emitting diodes by sidewall passivation using atomic layer deposition. *Optics Express*. 2018 Aug;26(16):21324.
- [34] Wong MS, Lee C, Myers DJ, Hwang D, Kearns JA, Li T, et al. Size-independent peak efficiency of III-nitride micro-light-emitting-diodes using chemical treatment and sidewall passivation. *Applied Physics Express*. 2019 Sep;12(9):097004.

Author Manuscript

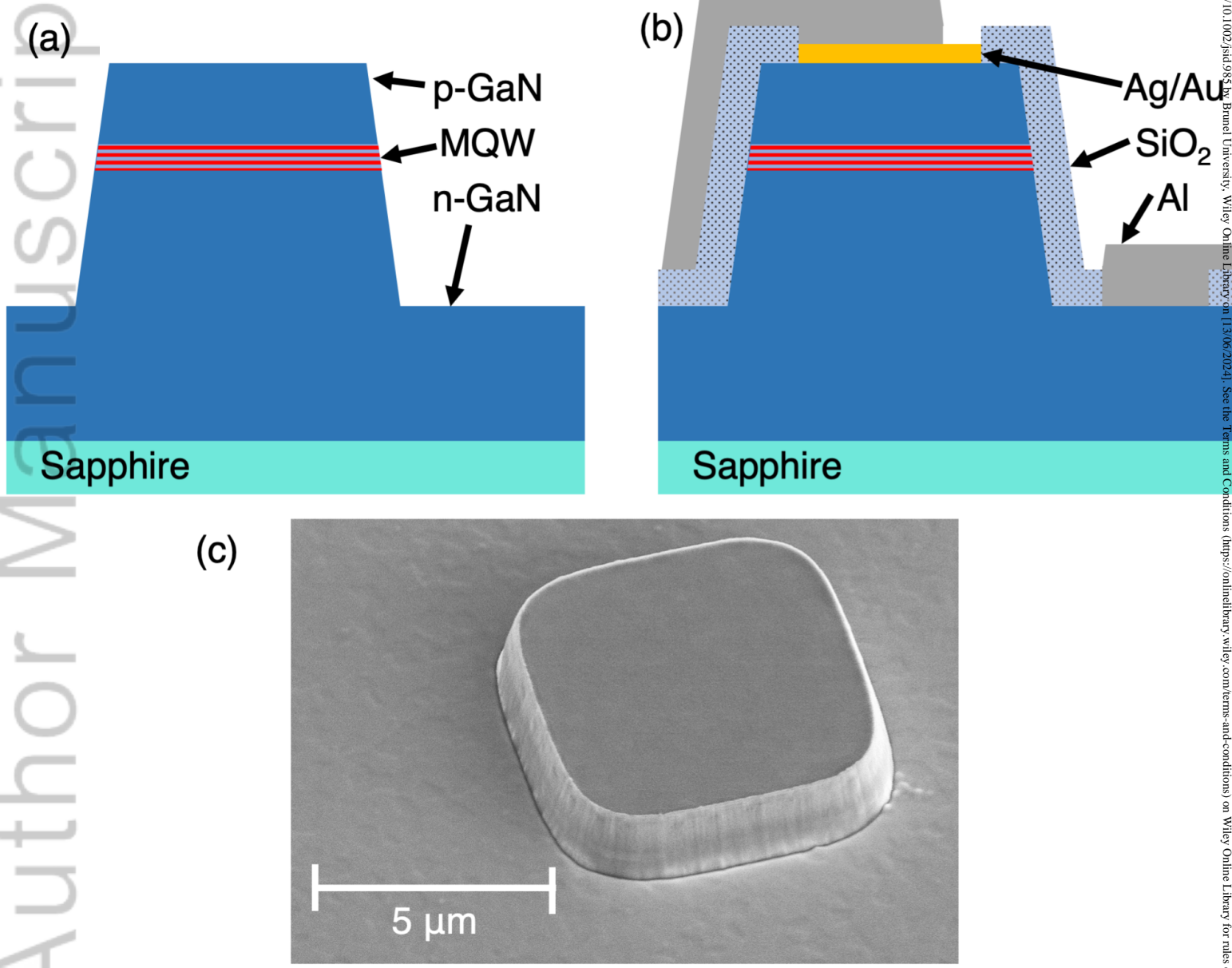


figure1.png

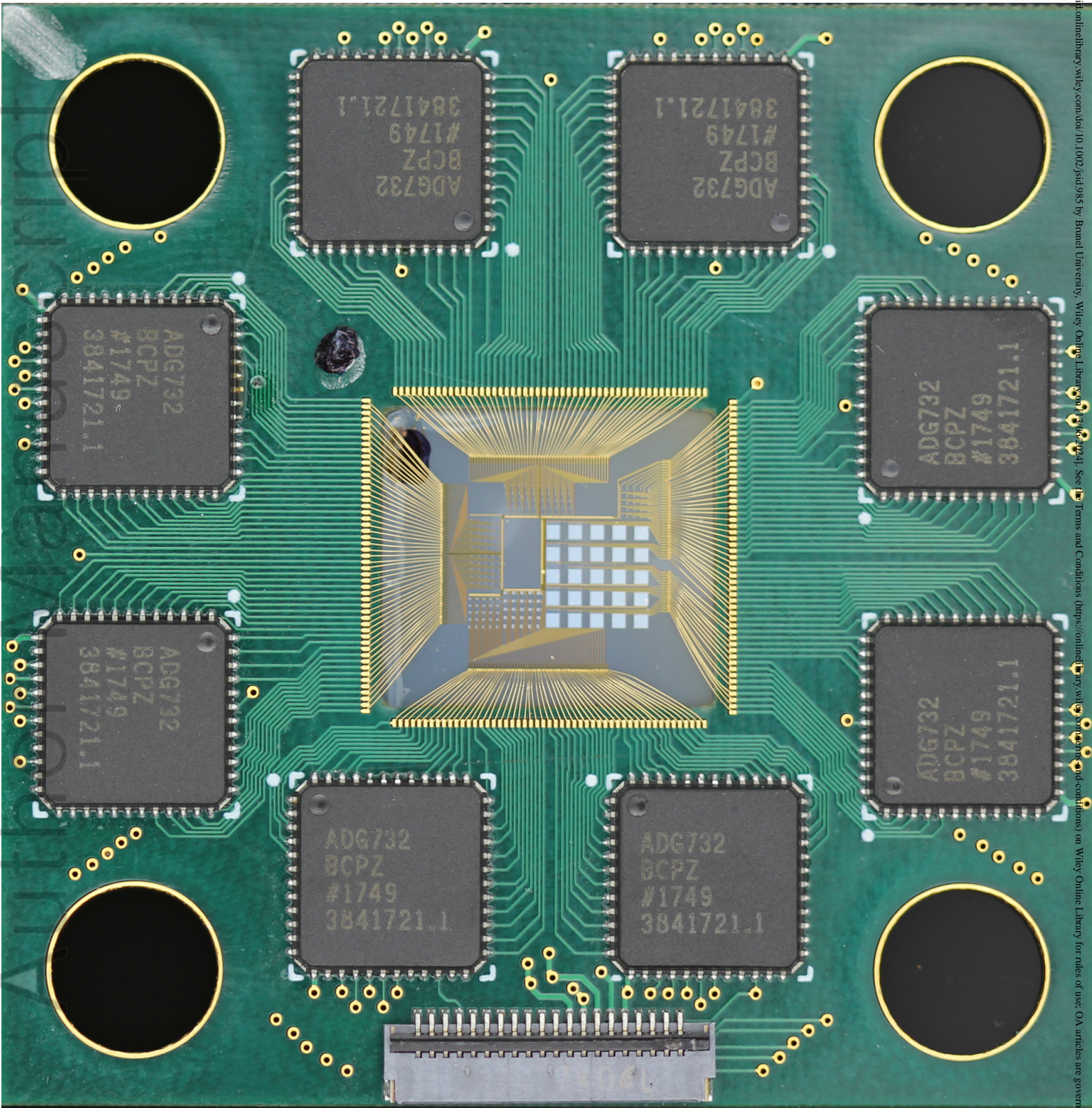


figure2.jpg



(a)

1 mm

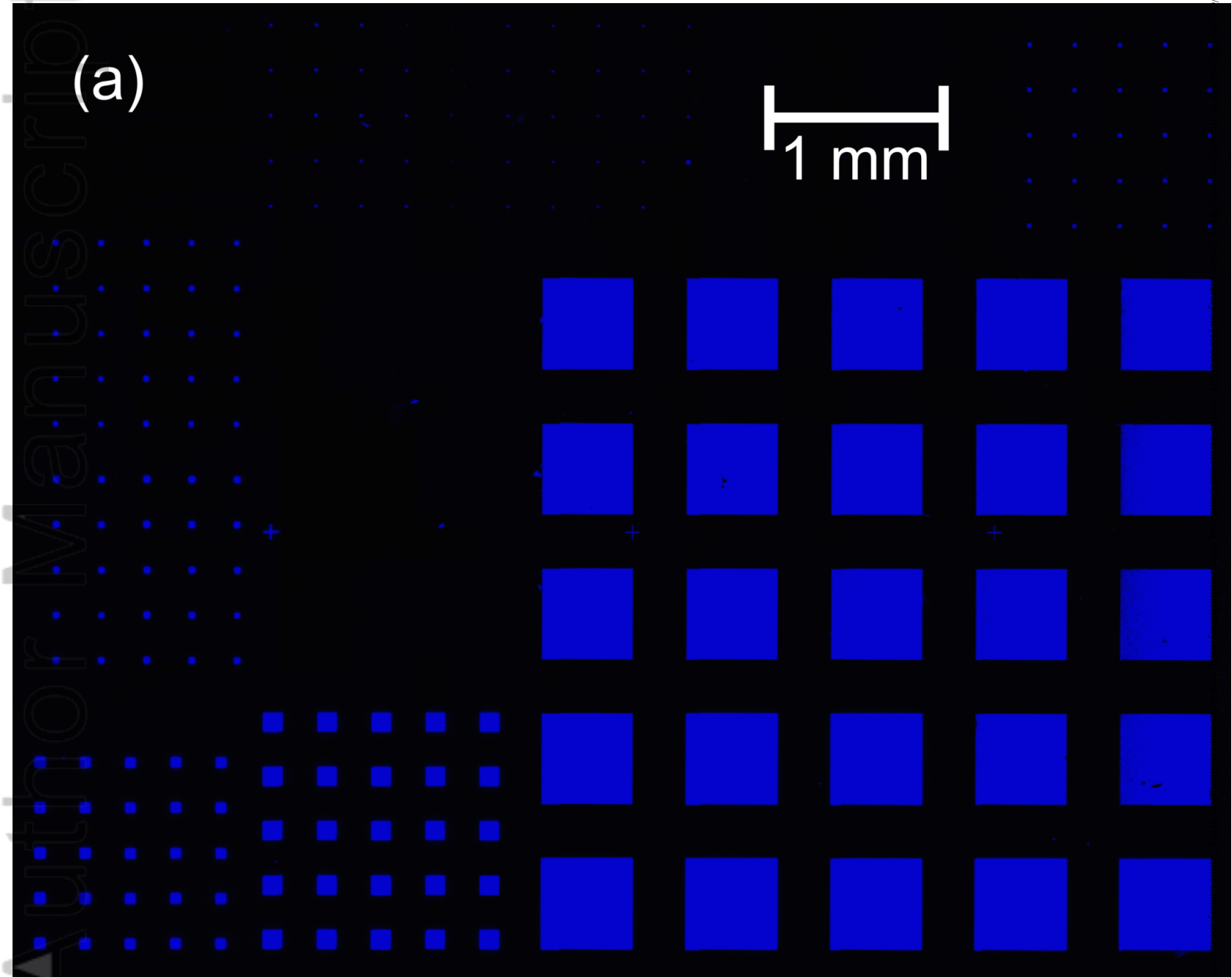


figure3a.png

(b)

1 mm

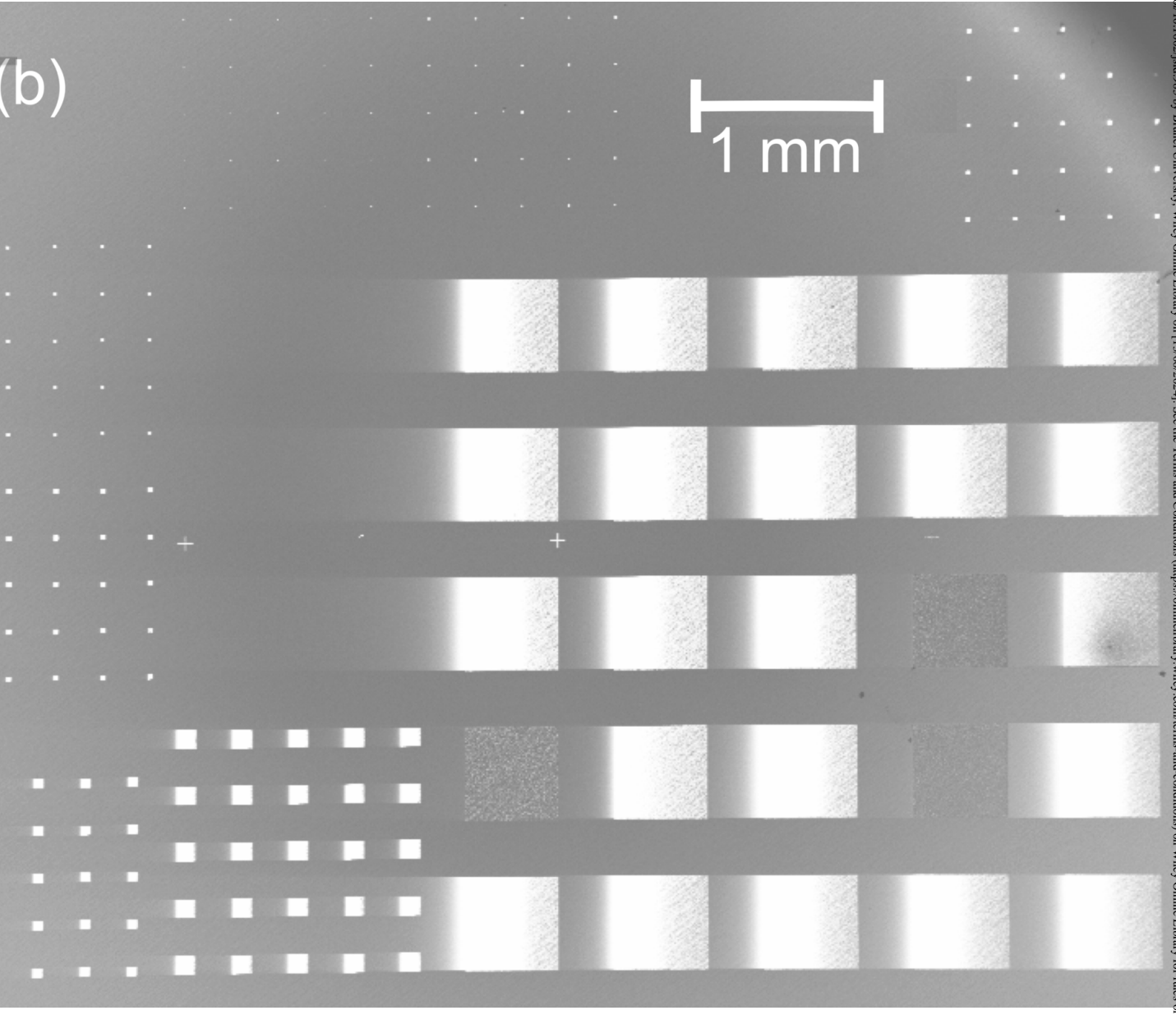


figure3b.png

Manuscript  
Author

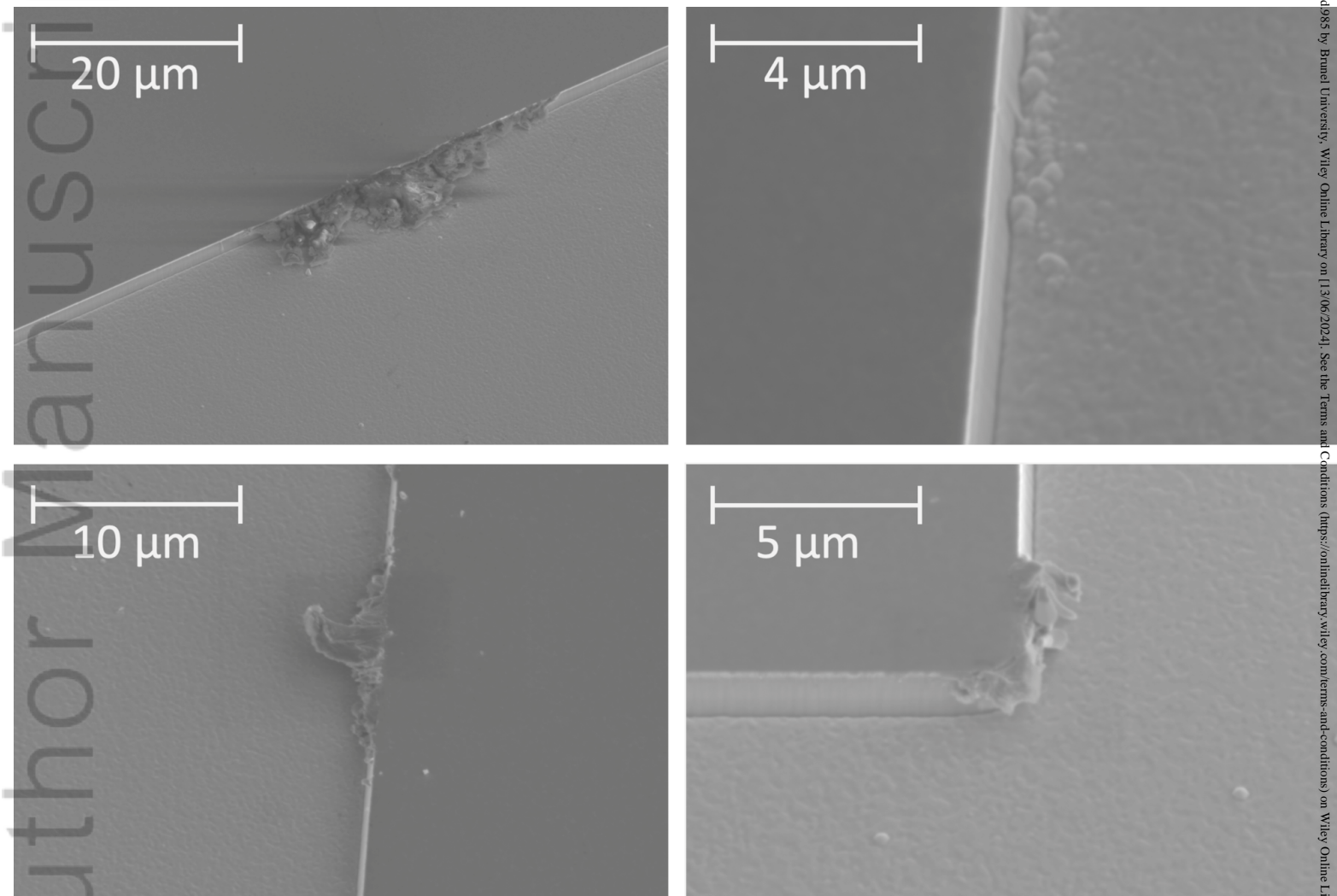
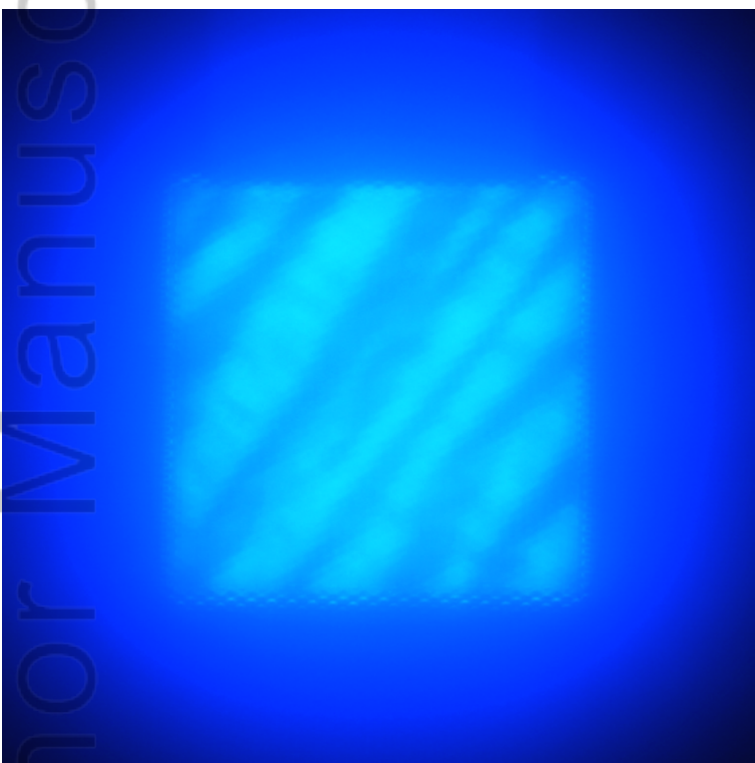
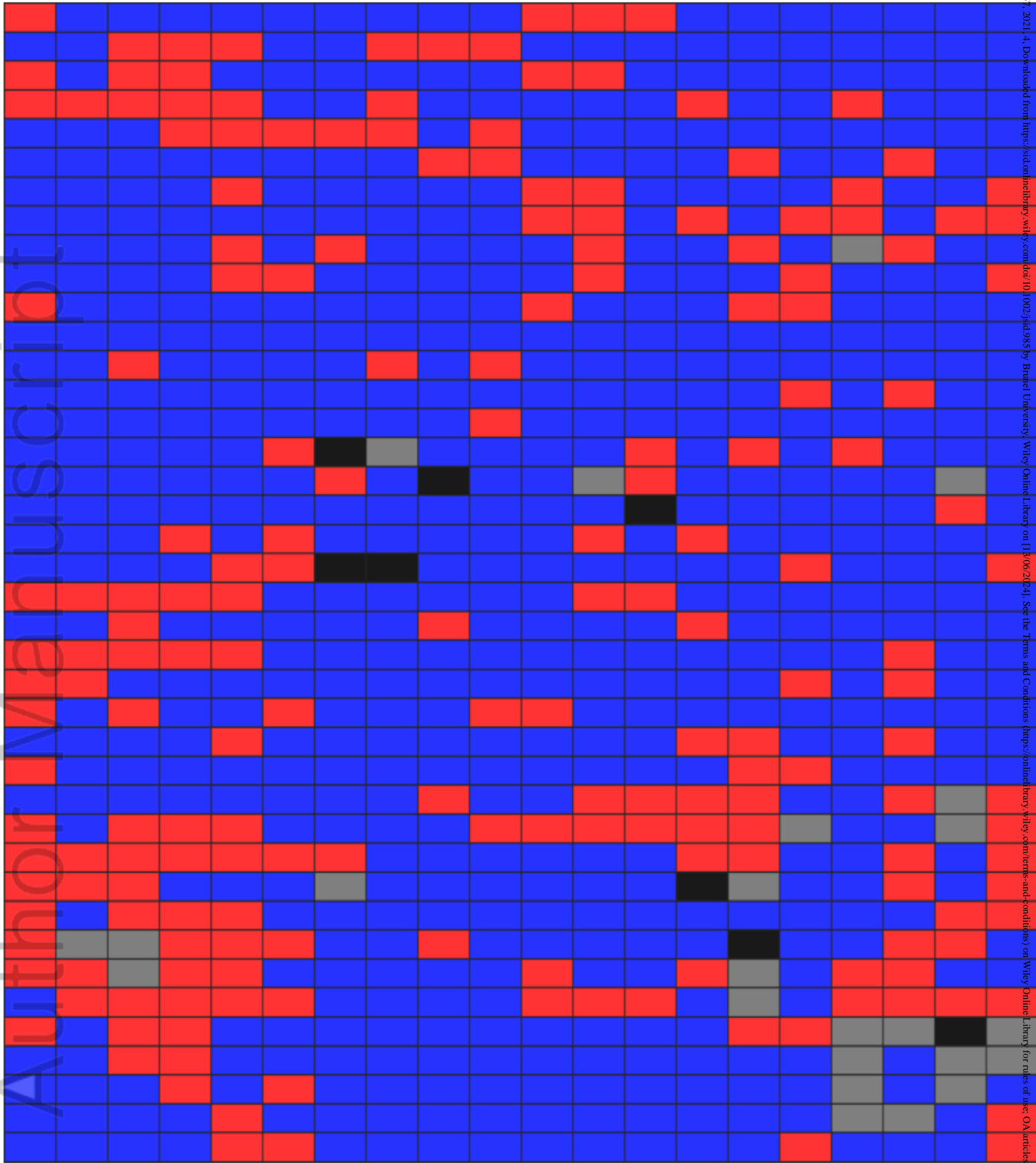






figure4.png



figure5.png





-  Emissive with cathodoluminescence and electroluminescence
-  Emissive with cathodoluminescence / inactive with electroluminescence
-  Inactive with cathodoluminescence and electroluminescence
-  Inactive with cathodoluminescence / emissive with electroluminescence

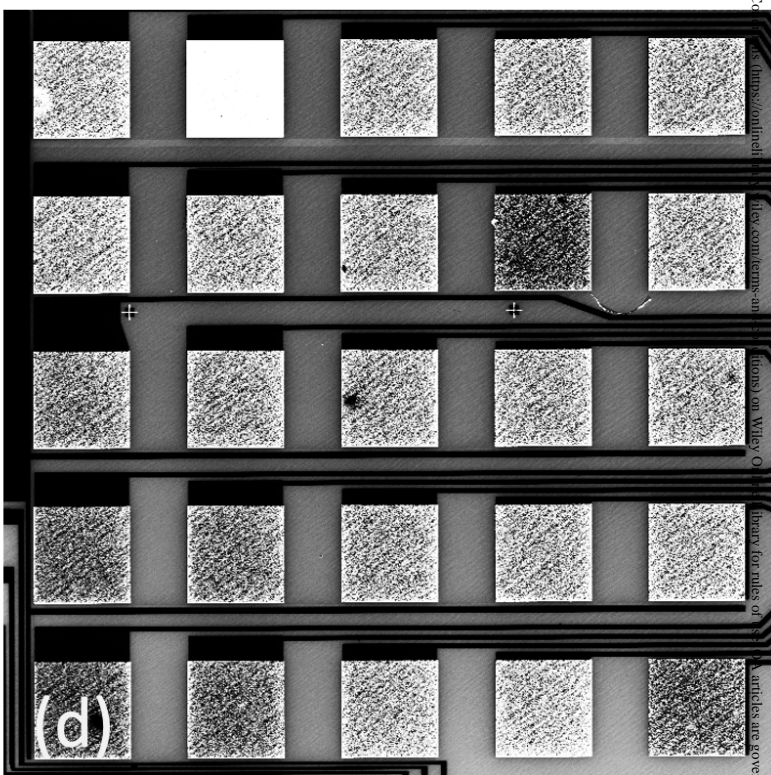
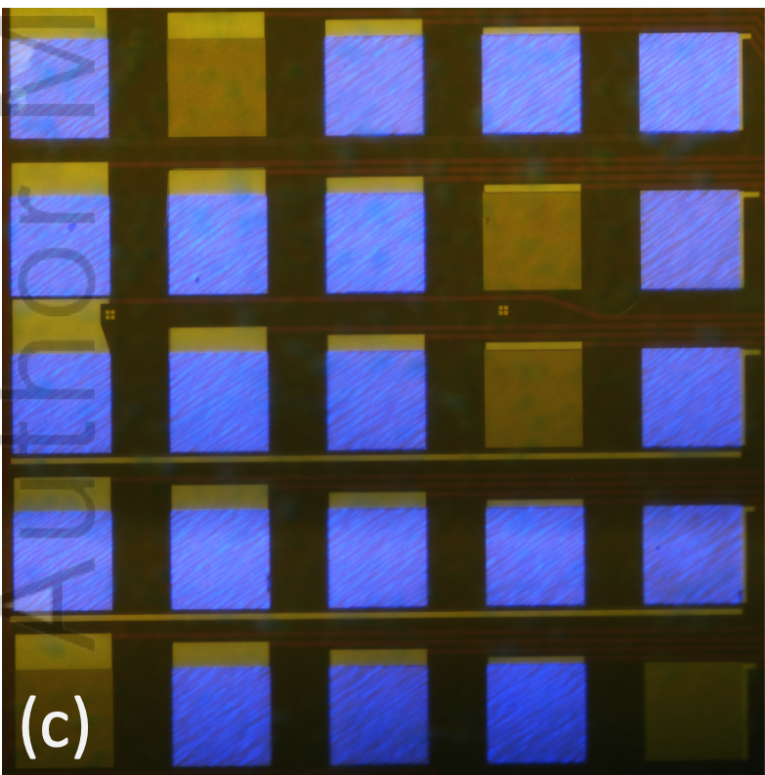
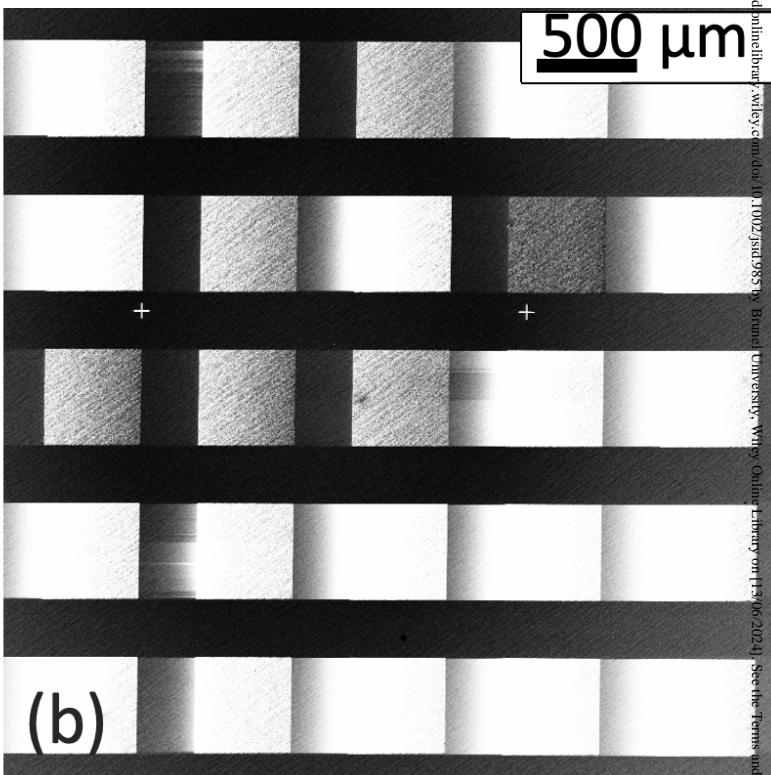
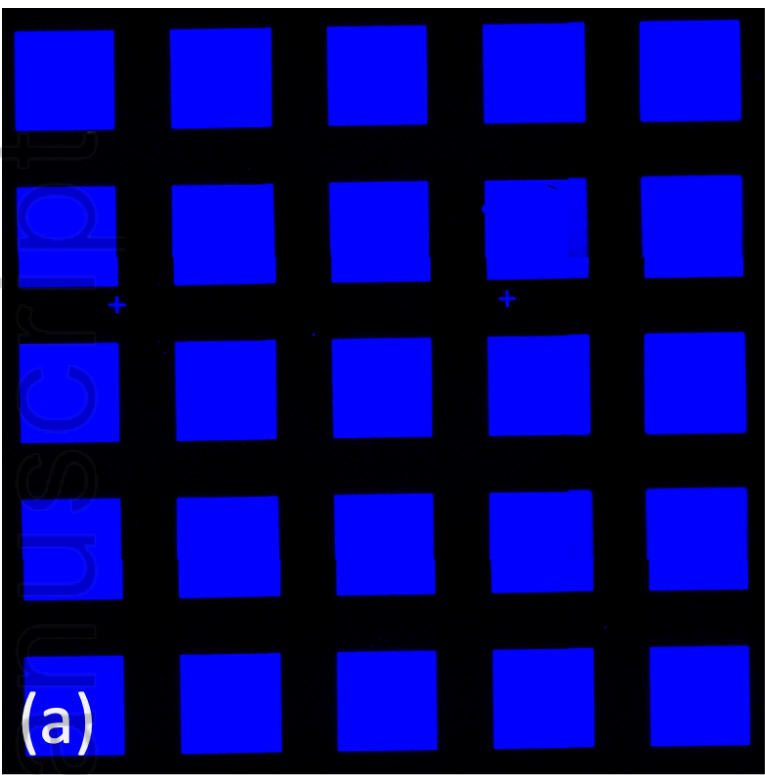


figure7.png

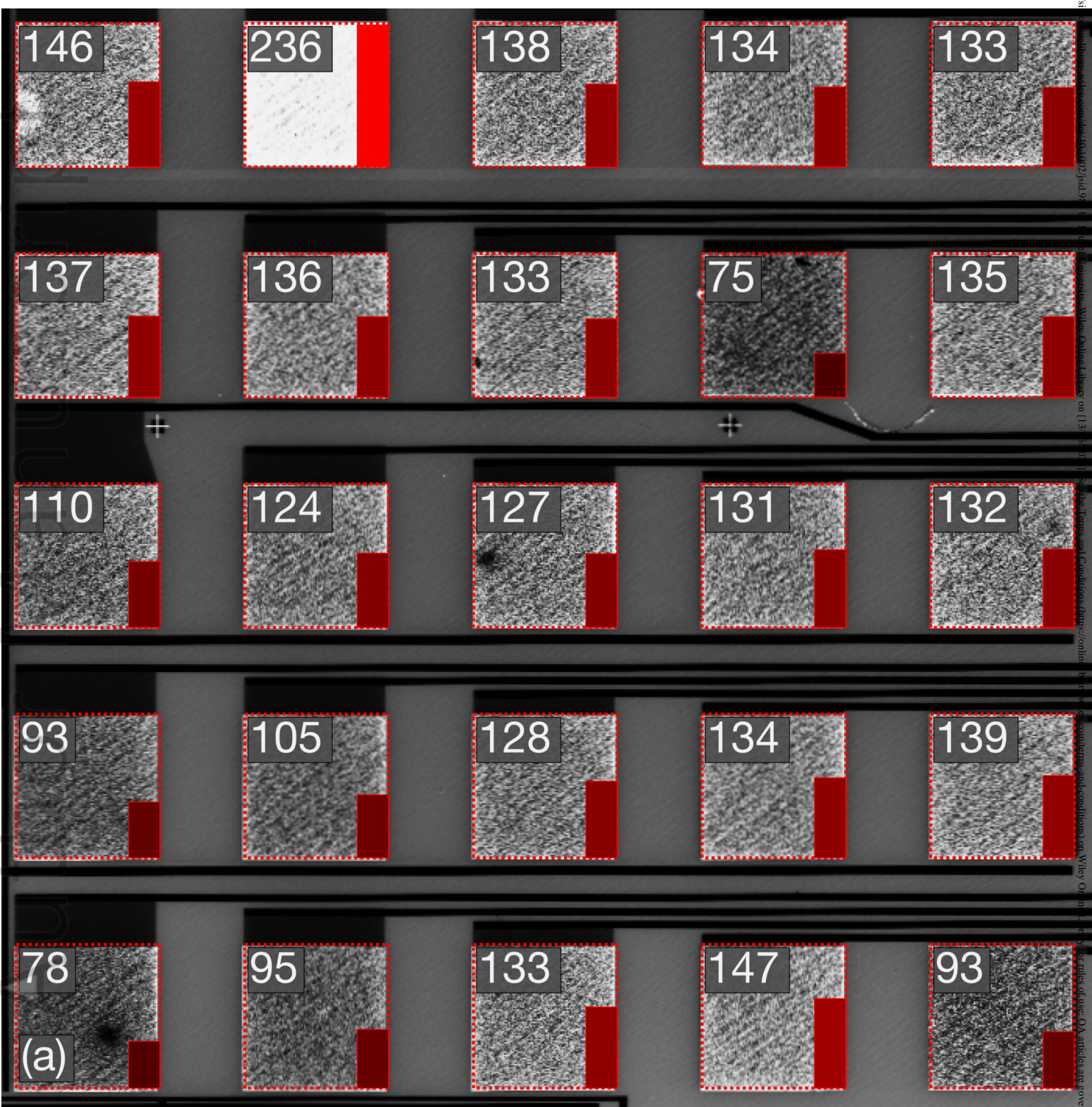


figure8a.png

Non-emissive

Emissive

(b)

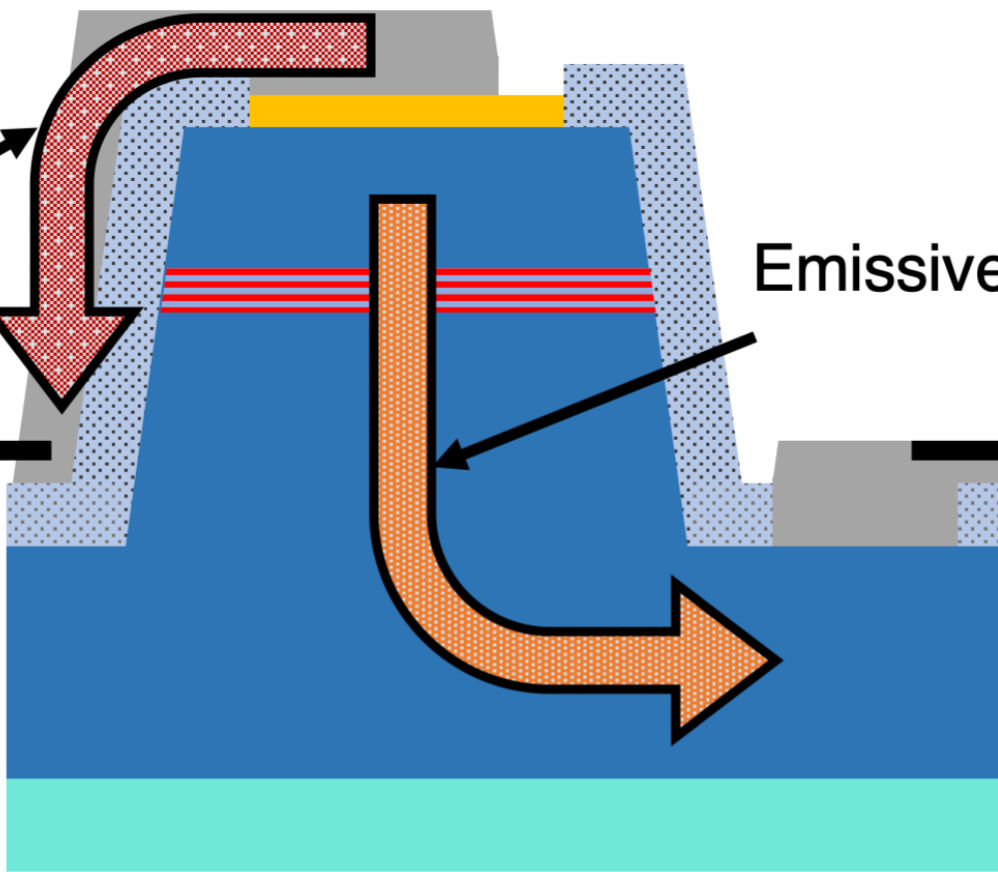
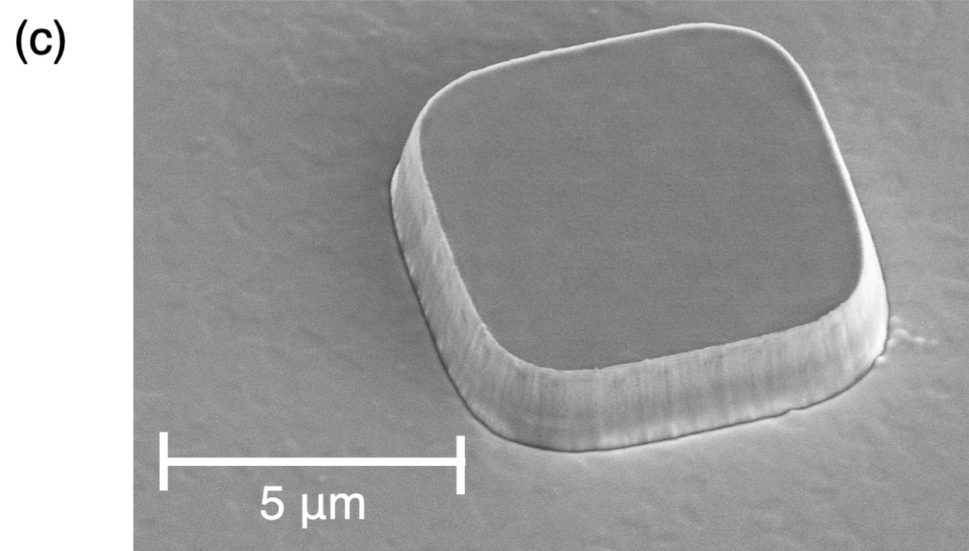
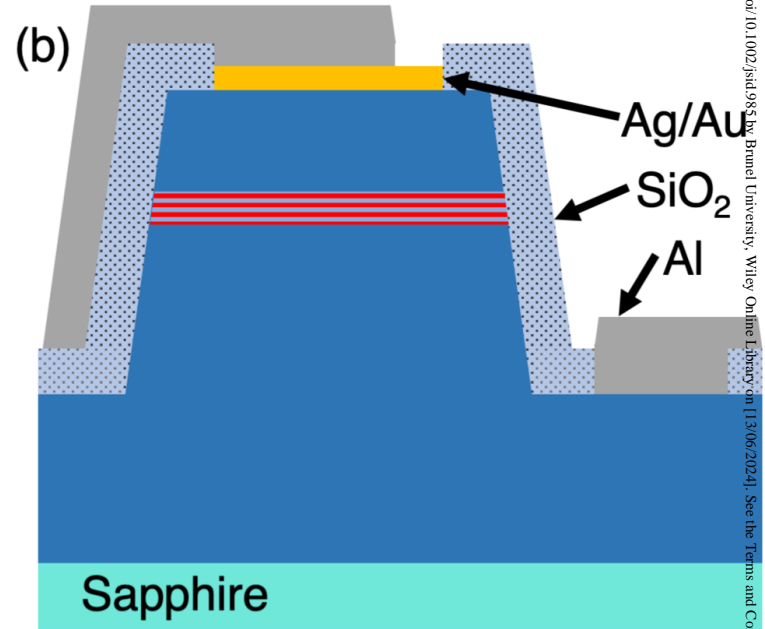
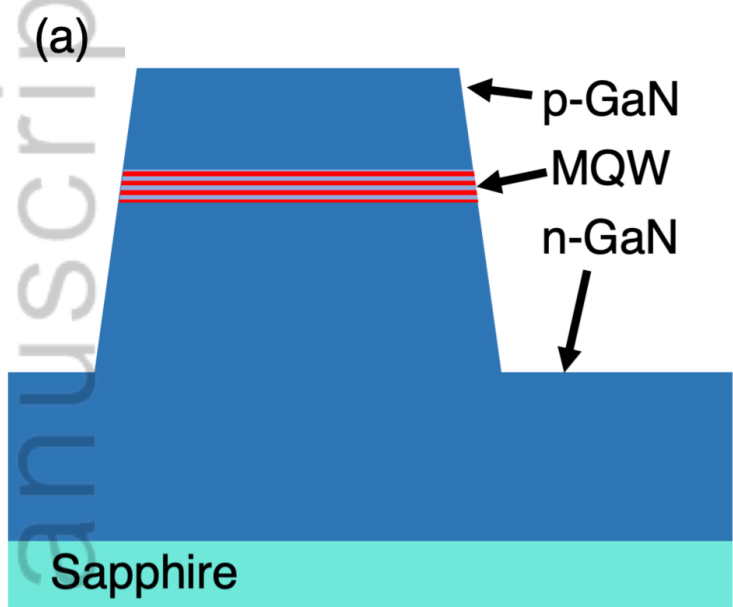


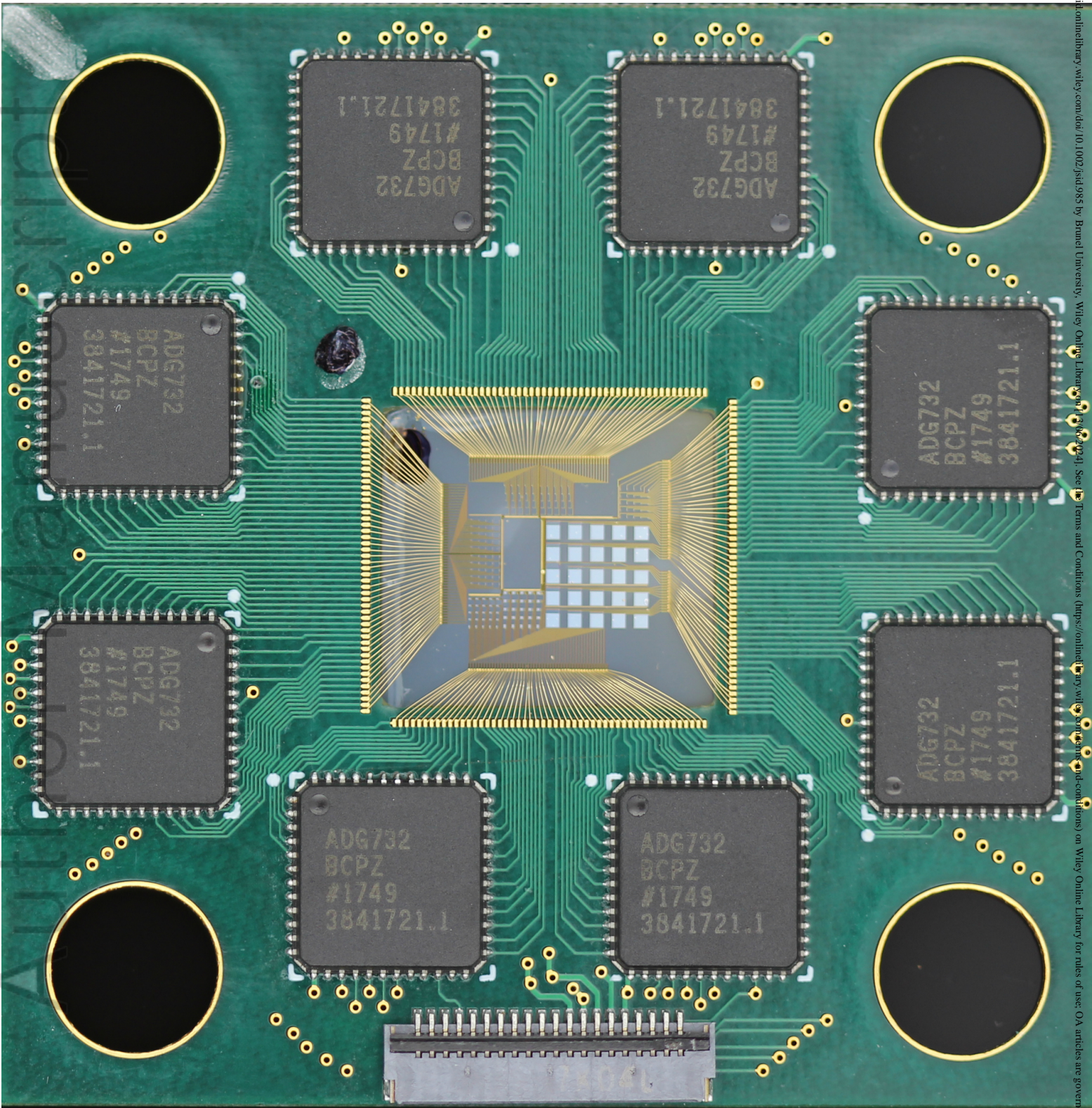
figure8b.png



Author Manuscript



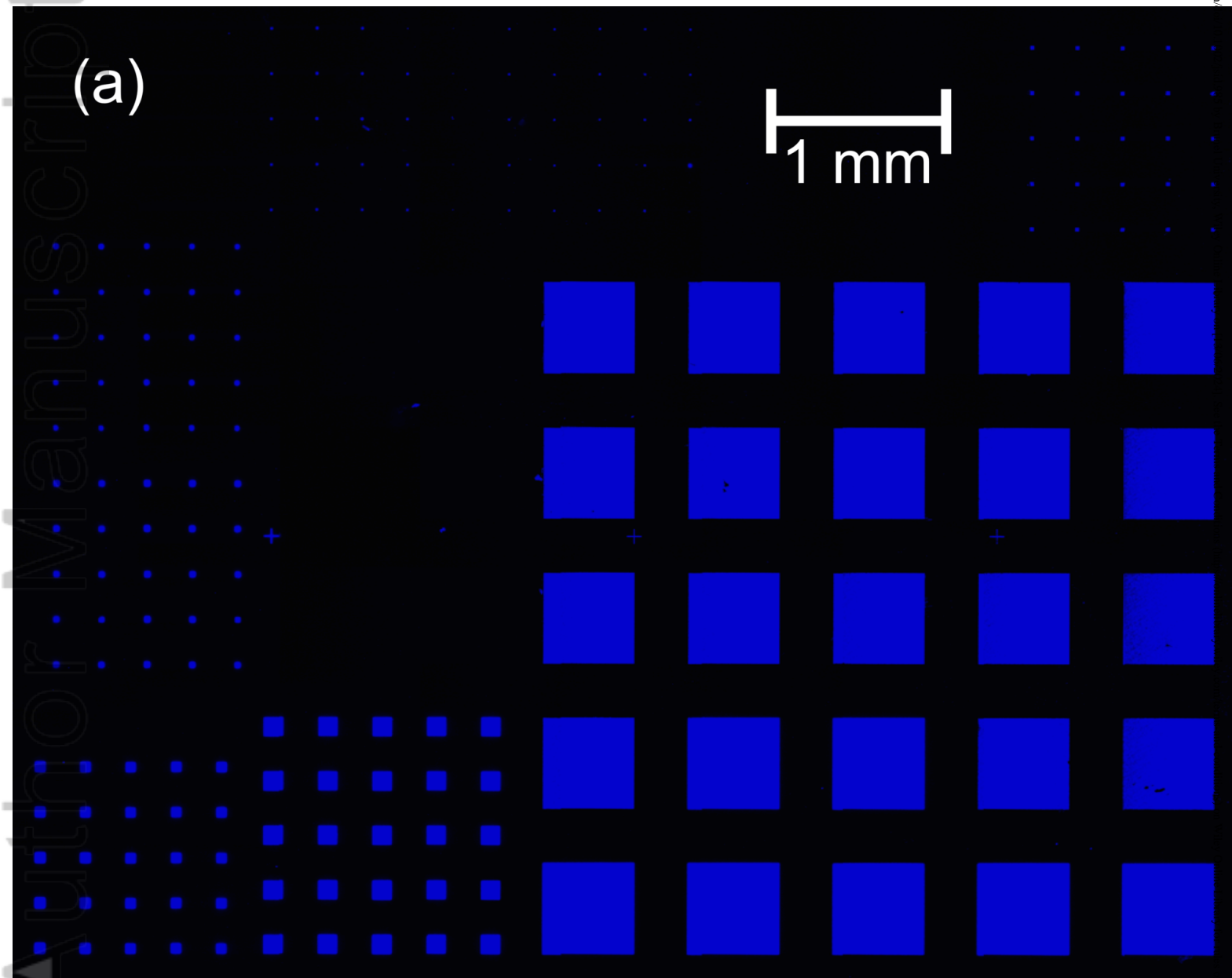
JSID\_985\_figure1.png



JSID\_985\_figure2.jpg

(a)

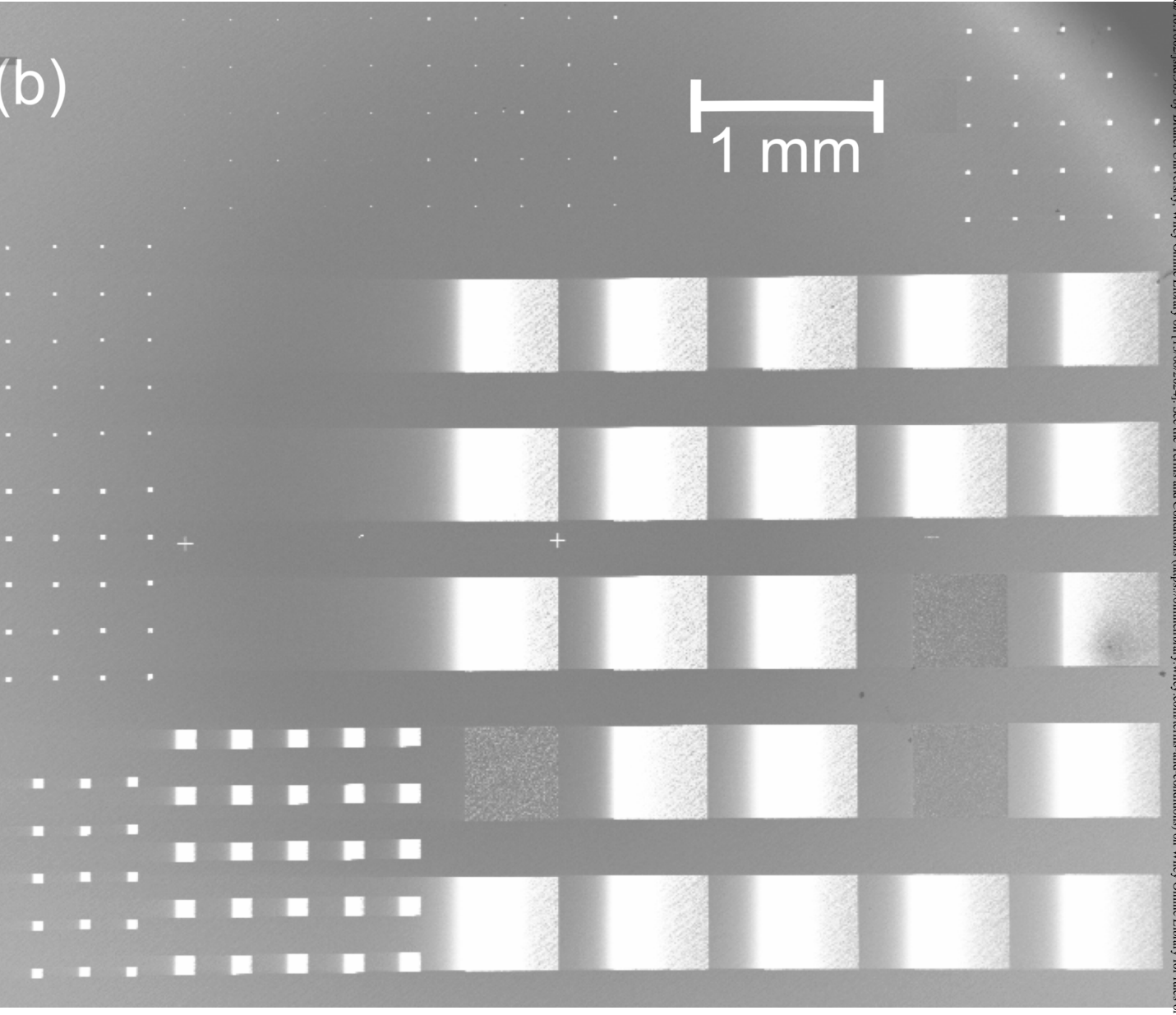
1 mm



JSID\_985\_figure3a.png

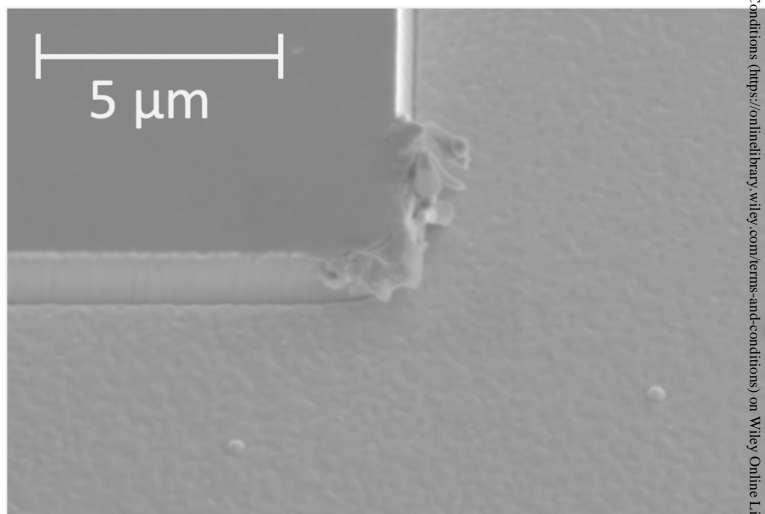
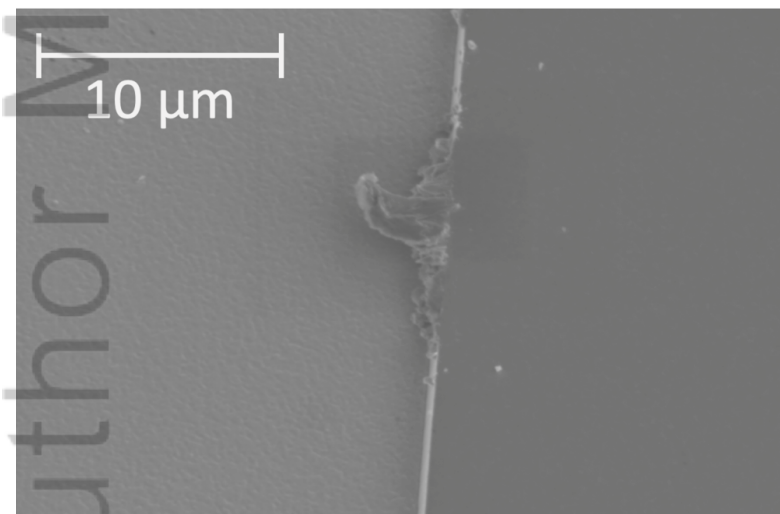
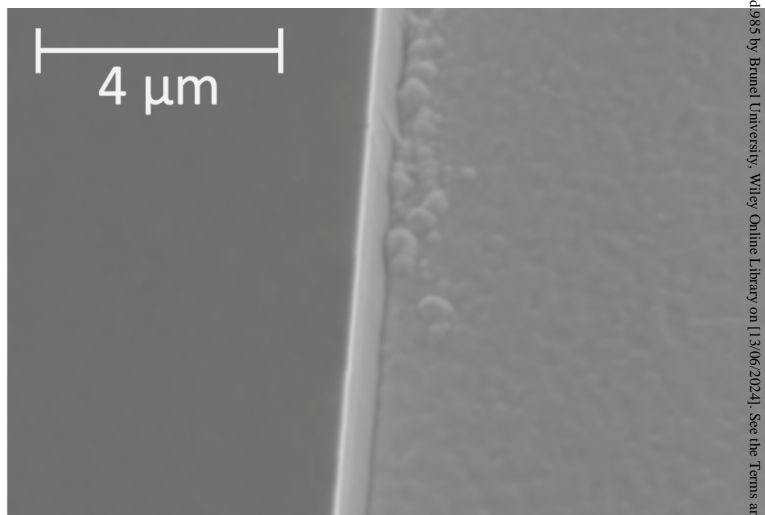
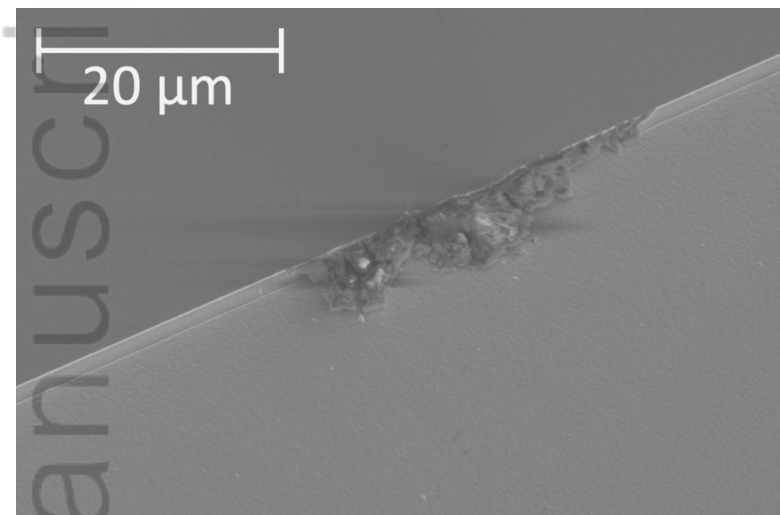
(b)

1 mm



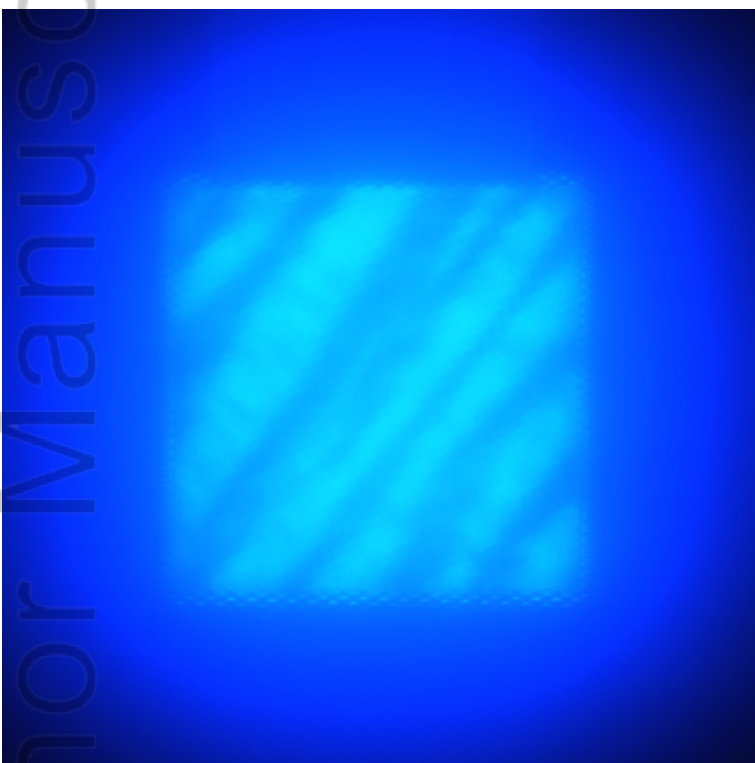
JSID\_985\_figure3b.png

Manuscript  
Author

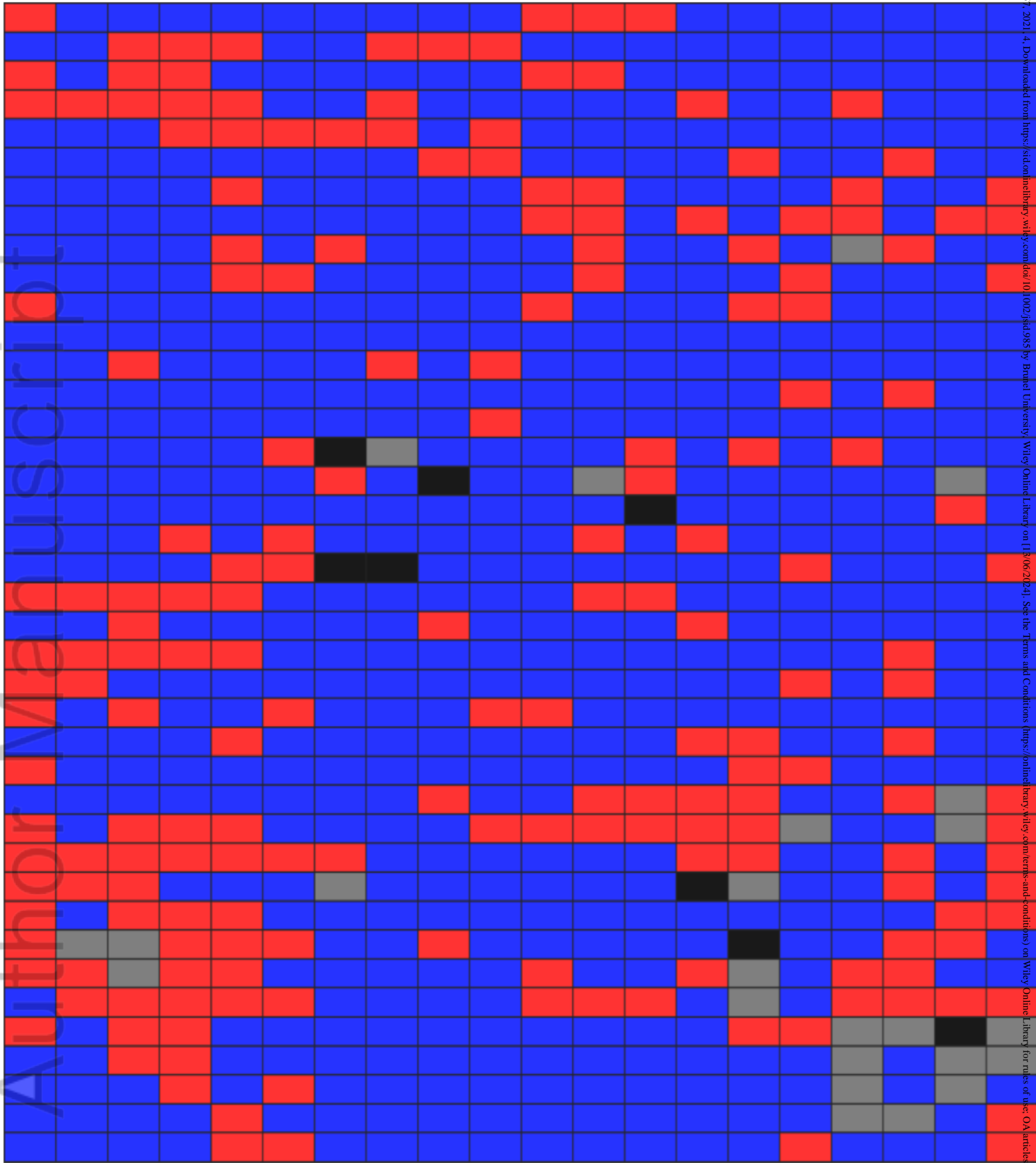






JSID\_985\_figure4.png

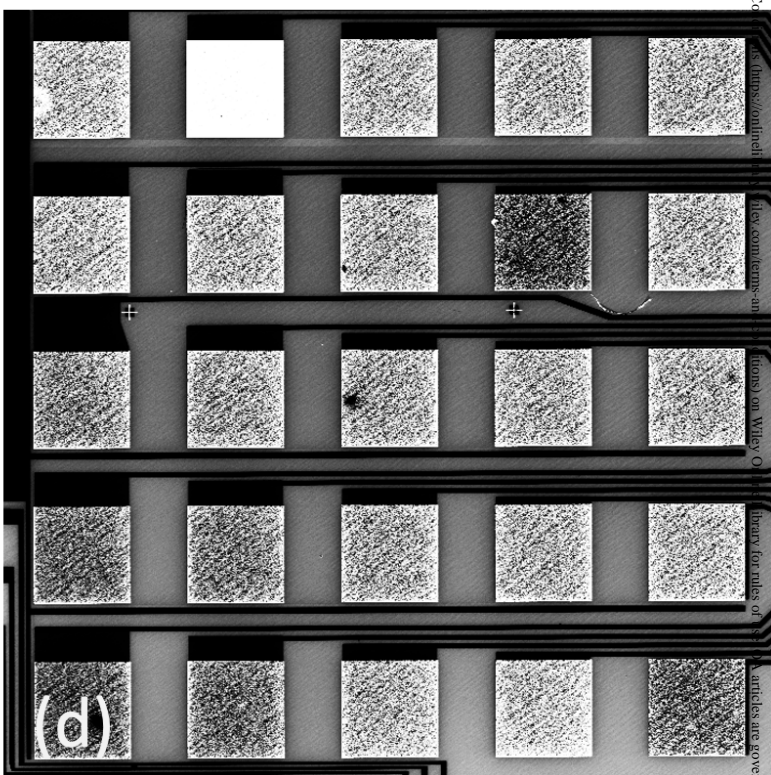
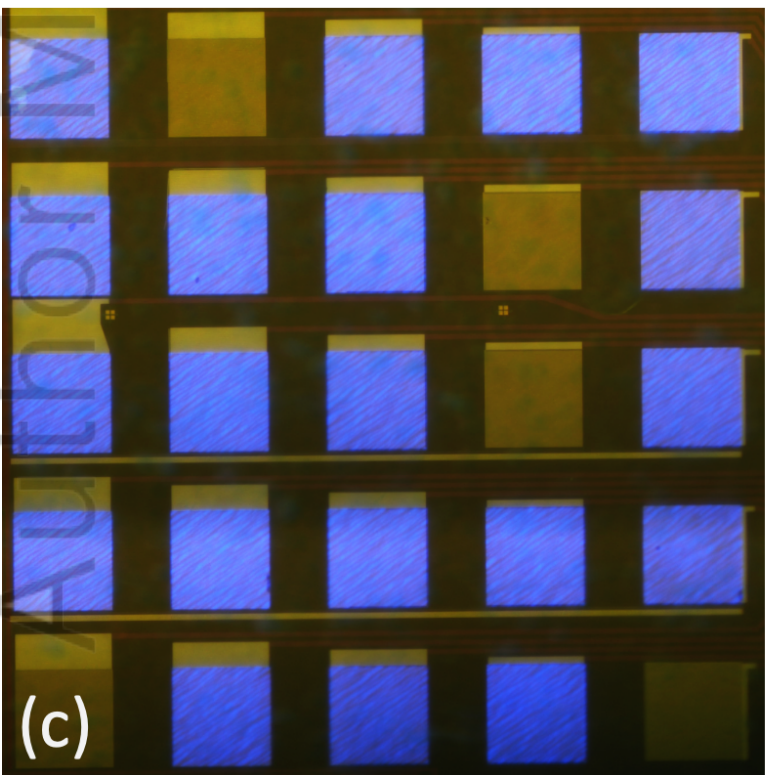
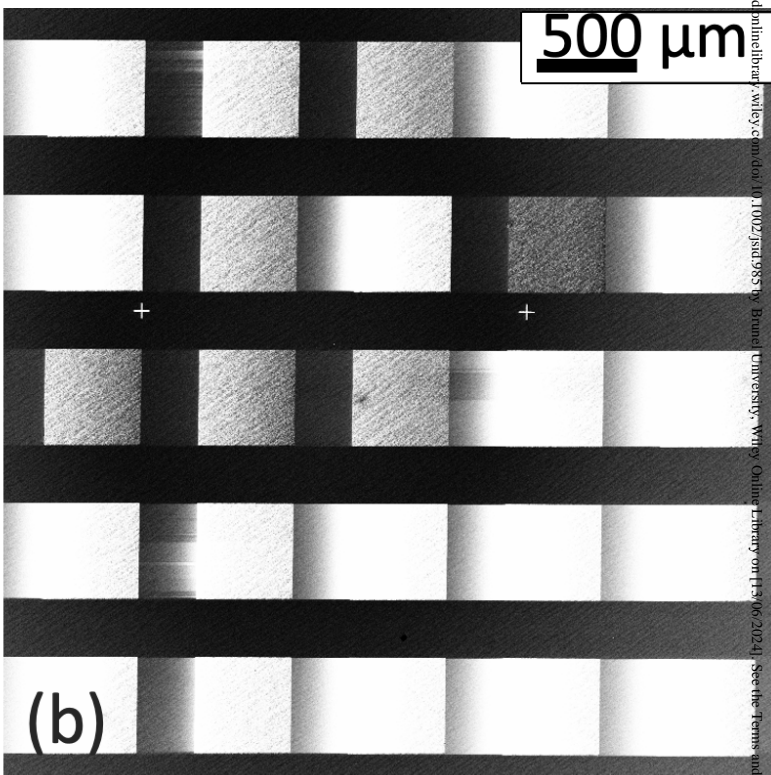
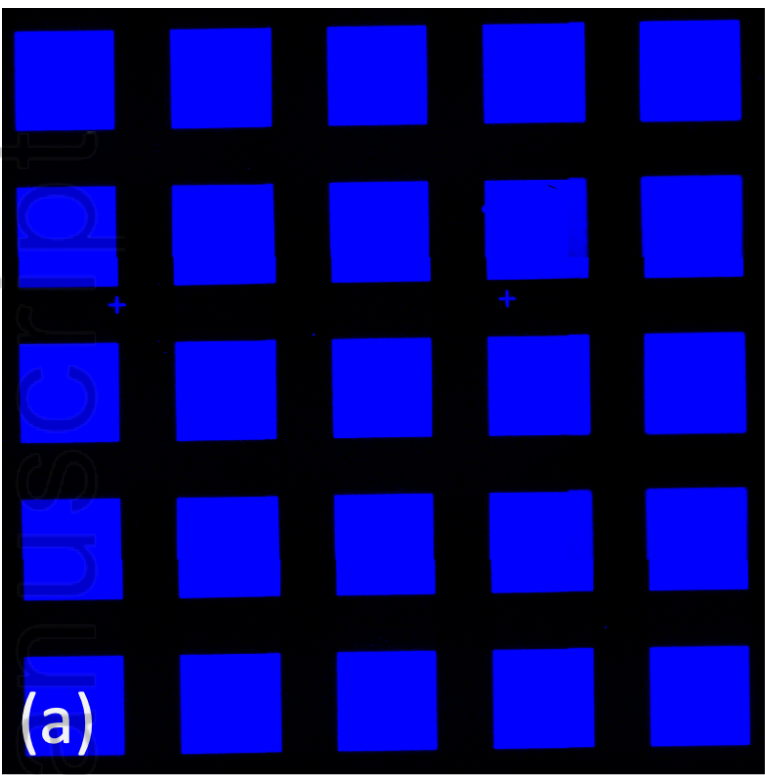
Author Manuscript



JSID\_985\_figure5.png

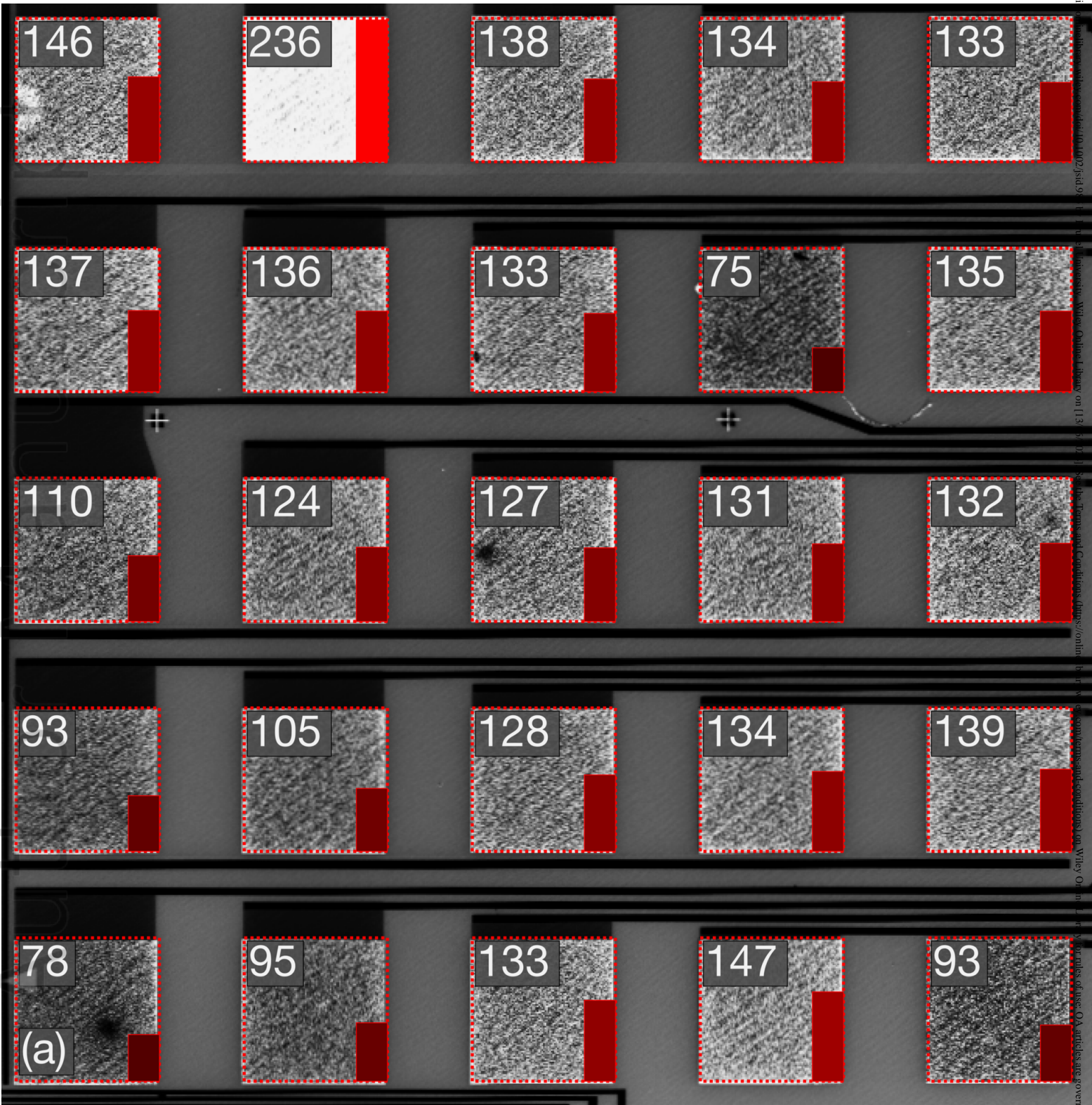


-  Emissive with cathodoluminescence and electroluminescence
-  Emissive with cathodoluminescence / inactive with electroluminescence
-  Inactive with cathodoluminescence and electroluminescence
-  Inactive with cathodoluminescence / emissive with electroluminescence



JSID\_985\_figure7.png



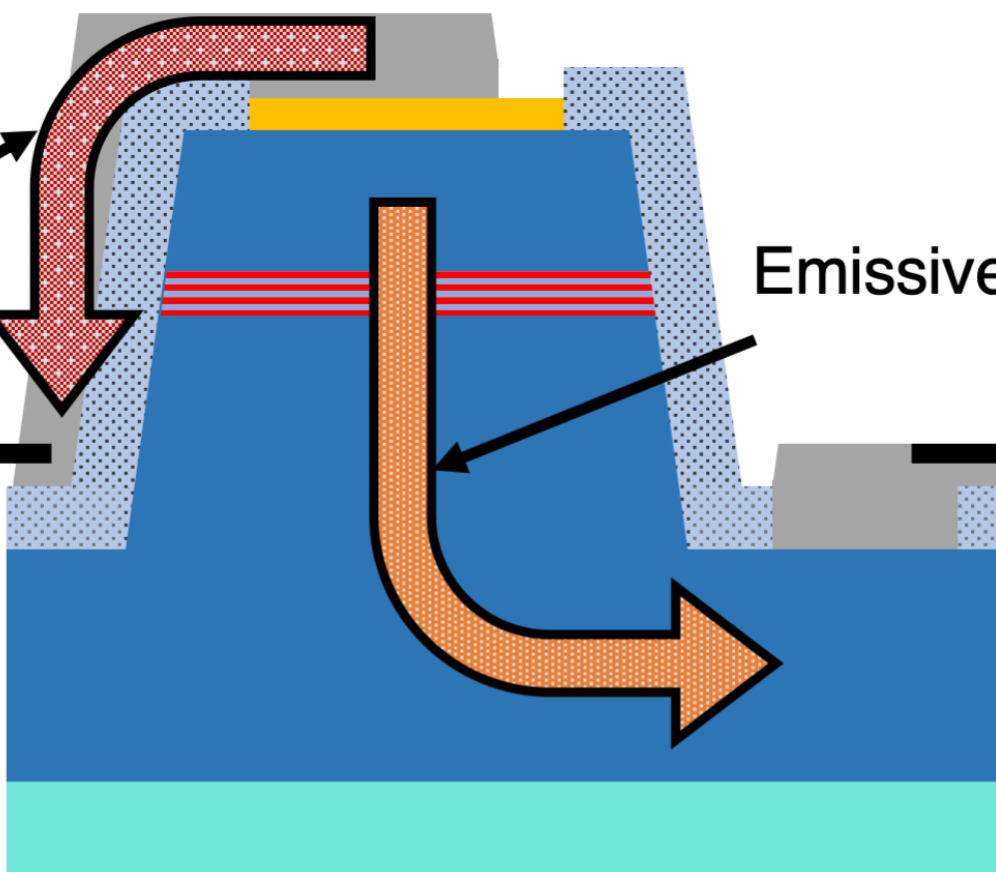


JSID\_985\_figure8a.png

Non-emissive

Emissive

(b)



JSID\_985\_figure8b.png